EUROFUSION WP15ER-PR(15) 14613

F Deluzet et al.

A DRIFT-ASYMPTOTIC SCHEME FOR A FLUID DESCRIPTION OF PLASMAS IN STRONG MAGNETIC FIELDS

Preprint of Paper to be submitted for publication in
Journal of Computational Physics

This work has been carried out within the framework of the EUROfusion Consortium and has received funding from the Euratom research and training programme 2014-2018 under grant agreement No 633053. The views and opinions expressed herein do not necessarily reflect those of the European Commission.

A DRIFT-ASYMPTOTIC SCHEME FOR A FLUID DESCRIPTION OF PLASMAS IN STRONG MAGNETIC FIELDS

FABRICE DELUZET*, MAURIZIO OTTAVIANI†, STEFAN POSSANNER*

ABSTRACT. In this work we present a numerical scheme for the ion Euler equations with Braginskii closure in the drift ordering of hot and strongly-magnetized plasmas. The scheme is constructed with the aid of asymptotic-preserving techniques and can be used on all time scales, ranging from the inverse cyclotron frequency to the time scales of plasma transport and ion drifts. There is no severe time step restriction related to the choice of time scale. Electrons are assumed adiabatic. The plasma is a three-dimensional slab in a uniform magnetic field. We use the ion-temperature-gradient dispersion relation for the scheme's verification. The promising results show that this could be a first step towards all-scale (all-speed) schemes for fluid tokamak simulations. Global plasma simulations could be envisioned, with the possibility of adapting the numerical parameters to the desired resolution.

1. INTRODUCTION

This work is about the numerical solution of the ion Euler equations with Lorentz force term in three space dimensions, henceforth called the Euler-Lorentz (EL) system, and written in dimensionless form:

$$(EL)\begin{cases} \dfrac{\partial n^\varepsilon}{\partial t} + \nabla\cdot\mathbf{\Gamma}^\varepsilon = 0\,, \\ \dfrac{\partial \mathbf{\Gamma}^\varepsilon}{\partial t} + \nabla\cdot\Big(\mathbf{\Gamma}^\varepsilon\otimes\dfrac{\mathbf{\Gamma}^\varepsilon}{n^\varepsilon}\Big) + \dfrac{1}{\varepsilon}\nabla p^\varepsilon + \nabla\cdot\Pi^\varepsilon_\wedge = \dfrac{1}{\varepsilon}\Big(n^\varepsilon\mathbf{E}^\varepsilon + \mathbf{\Gamma}^\varepsilon\times\mathbf{B}\Big)\,, \\ \dfrac{\partial w^\varepsilon}{\partial t} + \nabla\cdot\Big[\dfrac{\mathbf{\Gamma}^\varepsilon}{n^\varepsilon}(w^\varepsilon + p^\varepsilon)\Big] + \nabla\cdot\mathbf{q}^\varepsilon_\wedge = \mathbf{\Gamma}^\varepsilon\cdot\mathbf{E}^\varepsilon\,. \end{cases} \tag{1}$$

Here, n^ε stands for the ion density, $\mathbf{\Gamma}^\varepsilon = n^\varepsilon\mathbf{u}^\varepsilon$ is the ion flux ($\mathbf{u}^\varepsilon\in\mathbb{R}^3$ denoting the mean velocity), p^ε denotes the ion pressure and w^ε is the ion energy given by

$$w^\varepsilon = \frac{3}{2}n^\varepsilon T^\varepsilon + \varepsilon\frac{|\mathbf{\Gamma}|^2}{2n^\varepsilon}\,,\qquad p^\varepsilon = n^\varepsilon T^\varepsilon\,, \tag{2}$$

where T^ε denotes the ion temperature. The small parameter $\varepsilon\ll 1$ embodies the scaled Larmor radius as well as the squared Mach number, as precised in section 2. The magnetic field $\mathbf{B}$ is assumed to be given, with unit vector $\mathbf{b} := \mathbf{B}/|\mathbf{B}|$, which defines the local coordinates $\mathbf{x} = (\mathbf{x}_\perp, x_\parallel)$ as

$$(\mathbf{x}_\perp)_1 := [(Id - \mathbf{b}\otimes\mathbf{b})\mathbf{x}]_1\,,\qquad (\mathbf{x}_\perp)_2 := [(Id - \mathbf{b}\otimes\mathbf{b})\mathbf{x}]_2\,,\qquad x_\parallel := \mathbf{x}\cdot\mathbf{b}\,. \tag{3}$$

Date: November 3, 2015.

The electric field $\mathbf{E}^\varepsilon = -\nabla\phi^\varepsilon$ relates to the plasma density n^ε via the Boltzmann relation [38, 41], which together with the quasi-neutrality yields

$$\phi^\varepsilon = T_e \ln\left(\frac{n^\varepsilon}{n_c}\right), \qquad \text{where} \quad n_c = n_c(\mathbf{x}_\perp), \quad T_e = T_e(t, \mathbf{x}_\perp), \tag{4}$$

where ϕ^ε stands for the electrostatic potential; the equilibrium density n_c and the electron temperature T_e are assumed to be known and independent of the "parallel direction" $x_\parallel$. The terms $\Pi^\varepsilon_\wedge$ and $\mathbf{q}^\varepsilon_\wedge$ denote the gyro-viscous stress tensor and heat flux from the Braginskii closure of magnetized fluids [4, 35].

The purpose of this work is the development of a numerical scheme with uniform properties with respect to the scaling parameter ε. The main difficulty is related to the degeneracy of the momentum conservation law in the limit $\varepsilon \to 0$. To see this, let us define the parallel flux $\Gamma_\parallel \in \mathbb{R}$ and the perpendicular flux $\mathbf{\Gamma}_\perp \in \mathbb{R}^3$ via

$$\Gamma_\parallel := \mathbf{b}\cdot\mathbf{\Gamma}, \qquad \mathbf{\Gamma}_\perp := (Id - \mathbf{b}\otimes\mathbf{b})\mathbf{\Gamma}. \tag{5}$$

The notation (5) will be used for arbitrary vectors in $\mathbb{R}^3$ throughout this work, as well as for the gradient, $\nabla(\cdot) = \mathbf{b}\nabla_\parallel(\cdot) + \nabla_\perp(\cdot)$. Setting formally $\varepsilon = 0$ in the momentum conservation law in (1) leads to

$$\nabla_\parallel p^0 = n^0 E^0_\parallel, \qquad \nabla_\perp p^0 = n^0\mathbf{E}^0_\perp + \mathbf{\Gamma}^0_\perp \times \mathbf{B}_\perp. \tag{6}$$

In the limit regime, the perpendicular component of the momentum instantaneously adjusts in order to establish a zero force balance. The second relation can be solved for $\mathbf{\Gamma}^0_\perp$, yielding the "drift approximation"

$$\mathbf{\Gamma}^0_\perp = \frac{n^0\mathbf{E}^0\times\mathbf{B}}{|\mathbf{B}|^2} - \frac{\nabla_\perp p^0\times\mathbf{B}}{|\mathbf{B}|^2}. \tag{7}$$

The first term in (7) denotes the electric-field drift and the second term stands for the diamagnetic drift of the ions. The calculation of the perpendicular flux $\mathbf{\Gamma}^0_\perp$ in the limit $\varepsilon \to 0$ is thus readily achieved by equation (7).

The equilibrium is different along the magnetic field lines. In this direction, the pressure waves travel at an infinite speed in the limit $\varepsilon \to 0$ in order for the pressure gradient to balance the electric forces, securing by this mean the zero force regime. The computation of the parallel flux $\Gamma^0_\parallel$ in this low Mach regime is more intricate, since it has disappeared from the first equation in (6). A first part of this work will thus be dedicated to the derivation of an equation providing $\Gamma^0_\parallel$ whatever the regime. This is achieved thanks to a reformulation of the system providing an equivalent set of equations in which the drift limit is regular. This is a standard approach for asymptotic preserving methods, a class of numerical methods introduced at the beginning of the millennium [37] in the context of multi-scale kinetic equations [15, 16, 26, 29, 30, 44]. The concept has since been transported to other areas of multi-scale partial differential equations (PDEs) [17, 36]. Several AP-schemes have been developed in the context of fluid equations with for instance investigations of the quasi-neutral limit for plasma descriptions [11, 12, 21, 22], the reduced MHD [24] or, closer to the asymptotic adressed here, the low Mach number regime [9, 25, 45]. The present work is a

continuation of a series of papers devoted to the drift-fluid limit [6, 7, 19]. Two strategies have been introduced in these precedent realizations to overcome the degeneracy of the parallel momentum equation. One is close to the methodology of the low Mach number numerical methods, operating a wave equation in order to compute a pressure consistant with the force equilibrium along the magnetic field lines [7]. The second approach [6, 19], harness the parallel momentum as the Lagrange multiplier of the aligned force balance constraint. Both approaches entail the resolution of anisotropic wave or diffusion equations that degenerate in the drift limit. Indeed, in the $\varepsilon \to 0$ limit the diffusion along the magnetic line is infinite, and the computational domain being periodic, the dominant operator kernel is populated by the functions with a vanishing aligned gradient. This a common feature for the simulation of tokamak plasmas that has received a lot of attention [14], specifically by means of asymptotic preserving methods [3, 18, 23, 40].

The objective of the present work is to bring the concepts initiated in precedent realization to a richer framework in order to demonstrate the efficiency of the method and to perform the numerical method verification. The targeted phenomenology is the development of the Ion Temperature Gradient Instability (ITG) [10, 13] for which analytic estimates can be compared to the numerical method outputs. With this aim, the modelling used so far, in order to provide a proof of principle, has to be significantly complemented. First, the isotherm [6, 7] or isentropic [19] plasma descriptions are substituted by a full description of the ions, with an energy equation, furthermore the system incorporates Braginskii gyro-viscuous terms [4, 35] as mentioned above. The set up is also extended to a fully three dimensional configuration with, for sake of simplifying the numerical schemes, a magnetic field constant and align to one of the coordinates. The asymptotic-preserving reformulation of the system is thus reworked in this enriched framework. In the precedent realization [6, 7], the ill-posedness of the diffusion equation for vanishing ε is prevented thanks to a differential characterization of the dominant operator kernel space [8] that is not readily implemented for periodic geometries. In order to address accurately this property, the duality based method [18] is operated for the resolution of the reformulated system with a precision independent of the asymptotic parameter.

This article is organized as follows: in Section 2 the physical context of the plasma fluid model is precised, with the definition of the scaling assumptions leading to its dimensionless form. The asymptotic preserving reformulation is addressed in the Section 3 with the numerical scheme detailed in the Section 4. A stability analysis of the scheme is investigated by means of a Von Neumann analysis. Finally, Section 5 is devoted to the verification of the scheme, scanning through the characteristic plasma time scales, from the cyclotron period to the the drift wave period, which are well separated in fusion plasmas [34], with a particular attention brought to the intermediate regime characterizing the ITG growth.

2. Physical context and scaling

2.1. **Fluid equations for strongly magnetized plasmas.** The model investigated here is based on the Braginskii closure [4] for magnetized plasmas. Let m and Ze stand for the ion mass and charge, respectively, e denoting the elementary charge and $Z \in \mathbb{N}$. In

physical variables, the fluid system (1) reads

$$\begin{cases} \dfrac{\partial n}{\partial t} + \nabla \cdot \mathbf{\Gamma} = 0\,, \\ \dfrac{\partial \mathbf{\Gamma}}{\partial t} + \nabla \cdot \Big(\mathbf{\Gamma} \otimes \dfrac{\mathbf{\Gamma}}{n} \Big) + \dfrac{1}{m} \nabla p + \dfrac{1}{m} \nabla \cdot \Pi_\wedge = \dfrac{Ze}{m} \Big(n\mathbf{E} + \mathbf{\Gamma} \times \mathbf{B} \Big)\,, \\ \dfrac{\partial w}{\partial t} + \nabla \cdot \Big[\dfrac{\mathbf{\Gamma}}{n}(w+p) + \dfrac{\mathbf{\Gamma}}{n} \cdot \Pi_\wedge \Big] + \nabla \cdot \mathbf{q}_\wedge = Ze \mathbf{\Gamma} \cdot \mathbf{E}\,, \end{cases} \tag{8}$$

where the ion energy is given by

$$w = \frac{3}{2} p + \frac{m|\mathbf{\Gamma}|^2}{n}\,. \tag{9}$$

According to Braginskii [4,35], the gyro-viscous stress tensor reads

$$\Pi_\wedge := \frac{p}{2\omega_c} \cdot \frac{1}{2} \left\{ (\mathbf{b} \times \mathbf{W}_u) \cdot (Id + 3\mathbf{b} \otimes \mathbf{b}) + [(\mathbf{b} \times \mathbf{W}_u) \cdot (Id + 3\mathbf{b} \otimes \mathbf{b})]^t \right\}\,, \tag{10}$$

where ω_c denotes the ion cyclotron frequency and where $\mathbf{W}_u$ is the rate-of-strain tensor defined by

$$\mathbf{W}_u := \nabla \mathbf{u} + (\nabla \mathbf{u})^t - \frac{2}{3} (\nabla \cdot \mathbf{u})\, Id\,. \tag{11}$$

The gyro-viscous heat flux is given by

$$\mathbf{q}_\wedge := \frac{5}{2} \frac{nT}{m\omega_c} \mathbf{b} \times \nabla_\perp T\,. \tag{12}$$

These gyro-viscous terms are independent of the collisional regime and have to be included in fluid models of magnetized plasmas for the sake of a correct description of the drift limit. We elaborate on this in more detail when we study the cancellation of the diamagnetic drift terms in the linear, small-ε regime, c.f. section 4.2. Remark in particular that the model (8) is non-dissipative.

Due to the small mass ratio between electrons and ions, the electron dynamics is much faster than the ion dynamics. Thus, electron inertia can be rightfully neglected when studying large scale phenomena. This leads to the "Boltzmann relation" [41] along the magnetic field lines:

$$n_e(t, x_\parallel, \mathbf{x}_\perp) = n_c(\mathbf{x}_\perp) \exp\left[\frac{e\,\phi(t, x_\parallel, \mathbf{x}_\perp)}{k_B\, T_e(t, \mathbf{x}_\perp)} \right]\,. \tag{13}$$

Moreover, in this work we assume quasi-charge-neutrality, since we are not interested in plasma waves. Then, setting $n_e \approx n$ yields an equation for the electric potential,

$$\phi = \frac{k_B T_e}{e} \ln\Big(\frac{n}{n_c} \Big)\,. \tag{14}$$

Since we assume T_e and n_c to be given in what follows, Eq. (14) completes our model; it is to be solved self-consistently with the Eqs. (8), where the magnetic field is supposed to be known.

2.2. **Nondimensional model equations.** Let us now write the system (8) in dimensionless variables. This will be useful for identifying the physical regime we are interested in (drift ordering). We start by introducing a typical scale for all quantities. For instance, $\bar{n}$ stands for the plasma density scale, so that the physical plasma density writes $n = \bar{n}n'$ where $n' = n'(t, \mathbf{x})$ is of order one. We also denote by $\bar{x}$ and $\bar{t}$ the typical space and time scales we consider. The dimensionless fluid system completed with the potential equation reads

$$\begin{cases} \dfrac{\partial n'}{\partial t'} + \dfrac{\bar{t}\bar{u}}{\bar{x}}\nabla' \cdot \mathbf{\Gamma}' = 0\,, \\ \dfrac{\partial \mathbf{\Gamma}'}{\partial t'} + \dfrac{\bar{t}\bar{u}}{\bar{x}}\nabla' \cdot \Big(\mathbf{\Gamma}' \otimes \dfrac{\mathbf{\Gamma}'}{n'}\Big) + \dfrac{k_B\bar{T}}{m}\dfrac{\bar{t}}{\bar{u}\bar{x}}\nabla' p' + \dfrac{k_B\bar{T}}{m}\dfrac{\bar{t}}{\omega_c\bar{x}^2}\nabla' \cdot \Pi'_{\wedge} = \dfrac{Ze\bar{B}}{m}\bar{t}\Big(\dfrac{\bar{E}}{\bar{u}\bar{B}}n'\mathbf{E}' + \mathbf{\Gamma}' \times \mathbf{B}'\Big)\,, \\ \dfrac{\partial w'}{\partial t'} + \dfrac{\bar{t}\bar{u}}{\bar{x}}\nabla' \cdot \Big[\dfrac{\mathbf{\Gamma}'}{n'}(w' + p') + \dfrac{\bar{u}}{\omega_c\bar{x}}\dfrac{\mathbf{\Gamma}'}{n'} \cdot \Pi'_{\wedge}\Big] + \dfrac{k_B\bar{T}}{m}\dfrac{\bar{t}}{\omega_c\bar{x}^2}\nabla' \cdot \mathbf{q}'_{\wedge} = \dfrac{Ze\bar{B}}{m}\bar{t}\dfrac{m}{k_B\bar{T}}\dfrac{\bar{u}\bar{E}}{\bar{B}}\mathbf{\Gamma}' \cdot \mathbf{E}'\,, \\ \phi' = \dfrac{k_BT_e}{e\bar{\phi}}\ln\Big(\dfrac{n'}{n'_c}\Big)\,. \end{cases} \tag{15}$$

The following parameters will characterize the plasma regime under consideration:

$$v_{th} = \sqrt{\frac{k_B\bar{T}}{m}}\,, \qquad \omega_c = \frac{Ze\bar{B}}{m}\,, \qquad \rho_{th} = \frac{v_{th}}{\omega_c}\,. \tag{16}$$

Here, v_{th} stands for the ion thermal velocity, ω_c is the ion cyclotron frequency and ρ_{th} denotes the ion Larmor radius related to their thermal velocity. Our choice of scales for the independent variables is the following:

$$\bar{x} := L\,, \qquad \bar{t} := \frac{L^2}{v_{th}\rho_{th}}\,, \tag{17}$$

where L stands for a macroscopic length scale, for instance the large radius of a Tokamak vessel, and the time scale $\bar{t}$ is known as the "Bohm time". We now introduce the small parameter ε as the square of the ratio between the ion Larmor radius and the macroscopic length scale L, signifying that we are interested in strongly magnetized plasmas:

$$\varepsilon := \Big(\frac{\rho_{th}}{L}\Big)^2 \ll 1\,. \tag{18}$$

Furthermore, we relate the characteristic macroscopic velocity $\bar{u}$ to the chosen space and time scales, respectively, leading to

$$\bar{u} := \frac{\bar{x}}{\bar{t}} = v_{th}\frac{\rho_{th}}{L} = v_{th}\sqrt{\varepsilon}\,, \qquad \Longrightarrow \qquad \frac{\bar{u}}{v_{th}} = \sqrt{\varepsilon} \ll 1\,. \tag{19}$$

It becomes clear that the flow velocities we aim to observe are small compared to the thermal velocity; hence we are interested in the subsonic regime, characterized by a small

Mach number. In order to complete the scaling, we suppose

$$\bar{E} = \frac{\bar{\phi}}{\bar{x}}\,, \qquad \bar{E} = \bar{u}\bar{B}\,, \qquad k_B\bar{T} = e\bar{\phi}\,, \qquad \bar{T} = \bar{T}_e\,. \tag{20}$$

The assumptions (17)-(20) represent the so-called "drift-ordering" of the plasma fluid equations; applying them to system (15) and neglecting terms of order $\mathcal{O}(\varepsilon)$ in the energy equation yields the scaled Euler-Lorentz model (1), completed with the scaled potential equation (4). The primes will be omitted for clarity in the following.

3. Asymptotic-preserving reformulation

3.1. **General considerations.** In equation (6) we indicated that the drift limit $\varepsilon \to 0$ in the (EL)-model requires a reformulation of the momentum conservation law, in order to find the correct asymptotic equation for $\Gamma^\varepsilon_\parallel$. This reformulation is now presented in detail. It is based on the works on asymptotic-preserving (AP) schemes for isothermal fluid models summarized in [17] and implemented in [6, 7]. The reformulation is not unique, as several different approaches can be taken to "extract" the asymptotic behavior of $\Gamma^\varepsilon_\parallel$. Our aim is to formulate a wave equation for $\Gamma^\varepsilon_\parallel$ by using the mass conservation law. In the limit $\varepsilon \to 0$, the wave equation will degenerate to an elliptic problem along the field lines of $\mathbf{B}$. Depending on the boundary conditions, the elliptic problem has to be treated with care in order to yield a unique solution $\Gamma^0_\parallel$. We address the difficulty arising for periodic boundary conditions in the subsection 3.2 - "AP-formulation in a uniform $\mathbf{B}$-field".

Remark 1. *The following paragraphs clarify the AP reformulation of the (EL)-system* (1) *on the continuous level. We suggest that readers who are interested in the numerical scheme go directly to Section 4 and consult Section 3 where necessary, since the reformulation can be carried out (perhaps in a more intuitive way) also in the semi-discrete setting.*

Proposition 1. *Suppose that the (EL)-model* (1) *is posed with initial conditions* $(n^\varepsilon_0, \mathbf{\Gamma}^\varepsilon_0, w^\varepsilon_0)$, *and* $\mathbf{\Gamma}^\varepsilon_{\parallel,0}$ *is such that it satisfies the momentum conservation law at* $t = 0$. *Then, for* $\varepsilon > 0$, *an equivalent formulation of the (EL)-model is obtained when replacing the momentum conservation law with*

$$\begin{aligned}
&\varepsilon\frac{\partial^2\Gamma^\varepsilon_\parallel}{\partial t^2} - \nabla_\parallel\Big[(T^\varepsilon + T_e)\nabla_\parallel\Gamma^\varepsilon_\parallel\Big] - \nabla_\parallel\Big[(T^\varepsilon + T_e)(\Gamma^\varepsilon_\parallel\nabla\cdot\mathbf{b} + \nabla\cdot\mathbf{\Gamma}^\varepsilon_\perp)\Big] + \frac{\partial\mathbf{b}}{\partial t}\cdot\nabla\Big[(T^\varepsilon + T_e)n^\varepsilon\Big] \\
&\quad + \nabla_\parallel\left[n^\varepsilon\frac{\partial(T^\varepsilon + T_e)}{\partial t}\right] = \varepsilon\frac{\partial}{\partial t}\left(\mathbf{\Gamma}^\varepsilon\cdot\frac{\partial\mathbf{b}}{\partial t}\right) - \varepsilon\frac{\partial}{\partial t}\left\{\mathbf{b}\cdot\left[\nabla\cdot\left(\mathbf{\Gamma}^\varepsilon\otimes\frac{\mathbf{\Gamma}^\varepsilon}{n^\varepsilon} + \Pi^\varepsilon_\wedge\right)\right]\right\}\,, \qquad (21a)
\end{aligned}$$

$$\begin{aligned}
&\frac{\partial\mathbf{\Gamma}^\varepsilon_\perp}{\partial t} + \frac{\partial(\mathbf{b}\otimes\mathbf{b})}{\partial t}\,\mathbf{\Gamma}^\varepsilon + (Id - \mathbf{b}\otimes\mathbf{b})\nabla\cdot\left(\mathbf{\Gamma}^\varepsilon\otimes\frac{\mathbf{\Gamma}^\varepsilon}{n^\varepsilon} + \Pi^\varepsilon_\wedge\right) + \frac{1}{\varepsilon}\nabla_\perp(n^\varepsilon T^\varepsilon) \qquad (21b)\\
&\qquad\qquad = \frac{1}{\varepsilon}\Big(-n^\varepsilon\nabla_\perp\phi^\varepsilon + \mathbf{\Gamma}^\varepsilon_\perp\times\mathbf{B}\Big)\,,
\end{aligned}$$

Proof. Let us recall the notation introduced in (5) and thereafter. Applying the projection $(Id - \mathbf{b}\otimes\mathbf{b})$ on the momentum conservation law in (1) yields equation (21b). Taking the

scalar product of the momentum conservation law with the unit vector $\mathbf{b}$ yields

$$\frac{\partial \Gamma_\parallel^\varepsilon}{\partial t} - \mathbf{\Gamma}^\varepsilon \cdot \frac{\partial \mathbf{b}}{\partial t} + \mathbf{b} \cdot \left[\nabla \cdot \left(\mathbf{\Gamma}^\varepsilon \otimes \frac{\mathbf{\Gamma}^\varepsilon}{n^\varepsilon} \right) \right] + \frac{1}{\varepsilon} \nabla_\parallel (n^\varepsilon T^\varepsilon) + \mathbf{b} \cdot (\nabla \cdot \Pi_\wedge^\varepsilon) = -\frac{1}{\varepsilon} n^\varepsilon \nabla_\parallel \phi^\varepsilon \,. \quad (22)$$

Now, due to the Boltzmann relation (4), one has

$$n^\varepsilon \nabla_\parallel \phi^\varepsilon = \nabla_\parallel (T_e n^\varepsilon) \,, \quad (23)$$

such that the electric field term can be absorbed into the pressure gradient defined with the sum of the electronic and ionic temperatures $T^\varepsilon + T_e$. Then, differentiating (22) with respect to time, using $\partial_t \nabla_\parallel (\cdot) = \partial_t \mathbf{b} \cdot \nabla (\cdot) + \nabla_\parallel \partial_t (\cdot)$, further inserting into the pressure term the mass conservation law stated as

$$\frac{\partial n^\varepsilon}{\partial t} + \nabla \cdot (\mathbf{b} \Gamma_\parallel) + \nabla \cdot \mathbf{\Gamma}_\perp^\varepsilon = 0 \,, \quad (24)$$

and multiplying by ε leads to equation (21a).

Suppose now that $\varepsilon > 0$ and $\Gamma_\parallel^\varepsilon$ is a solution of (21a). Integrating this equation with respect to time in the interval $[0, s]$, and using that $\Gamma_\parallel^\varepsilon$ satisfies (22) at $t = 0$ (according to our assumption), it follows that $\Gamma_\parallel^\varepsilon$ satisfies (22) also at $t = s$. Thus it is also solution of the original momentum conservation law. Conversely, any solution of (22) satisfies (21a) by construction. □

We recognize that the first two terms in equation (21a) form a wave equation along the magnetic field lines with wave speed $\sqrt{(T^\varepsilon + T_e)/\varepsilon}$. In the drift limit $\varepsilon \to 0$ information thus propagates with infinite speed along the field lines, and $\Gamma_\parallel^0$ is determined from an elliptic equation:

$$\begin{aligned} -\nabla_\parallel \Big[(T^0 + T_e) \nabla_\parallel \Gamma_\parallel^0 \Big] - \nabla_\parallel \Big[(T^0 + T_e) (\Gamma_\parallel^0 \nabla \cdot \mathbf{b} + \nabla \cdot \mathbf{\Gamma}_\perp^0) \Big] \\ = -\frac{\partial \mathbf{b}}{\partial t} \cdot \nabla \Big[(T^0 + T_e) n^0 \Big] - \nabla_\parallel \left[n^0 \frac{\partial (T^0 + T_e)}{\partial t} \right] \end{aligned} \quad (25)$$

Owing to (24), the equation (25) is equivalent to $\partial_t \nabla_\parallel [(T^0 + T_e) n^0] = 0$. Supposing that $\nabla_\parallel [(T^0 + T_e) n^0]|_{t=0} = 0$ we obtain that the force balance relation (6) along the field lines is satisfied at all times. The reformulation in Proposition 1 thus yields the correct limit solution and moreover permits the calculation of $\Gamma_\parallel^0$, provided that (25) has a unique solution. We will address this point in the following subsection.

Another formulation can be stated instead of a wave equation, namely an integro-differential equation. It mimics the equation constructed thanks to a time semi-discretization and is thus more representative of the equations implemented in the numerical method.

Proposition 2. *For $\varepsilon > 0$, an equivalent formulation of the (EL)-model* (1) *is obtained when replacing the momentum conservation law with*

$$\varepsilon\frac{\partial\Gamma^\varepsilon_\parallel}{\partial t} - \nabla_\parallel\Big[(T^\varepsilon+T_e)\int_0^t \nabla_\parallel\Gamma^\varepsilon_\parallel(s)\,ds\Big] - \nabla_\parallel\Big[(T^\varepsilon+T_e)\int_0^t(\Gamma^\varepsilon_\parallel\nabla\cdot\mathbf{b}+\nabla\cdot\mathbf{\Gamma}^\varepsilon_\perp)(s)\,ds\Big]$$
$$= -\nabla_\parallel\Big[(T^\varepsilon+T_e)n^\varepsilon_0\Big] + \varepsilon\mathbf{\Gamma}^\varepsilon\cdot\partial_t\mathbf{b} - \varepsilon\mathbf{b}\cdot\left[\nabla\cdot\Big(\mathbf{\Gamma}^\varepsilon\otimes\frac{\mathbf{\Gamma}^\varepsilon}{n^\varepsilon}+\Pi^\varepsilon_\wedge\Big)\right], \tag{26a}$$

$$\frac{\partial\mathbf{\Gamma}^\varepsilon_\perp}{\partial t} - \frac{\partial(\mathbf{b}\otimes\mathbf{b})}{\partial t}\mathbf{\Gamma}^\varepsilon + (Id-\mathbf{b}\otimes\mathbf{b})\nabla\cdot\Big(\mathbf{\Gamma}^\varepsilon\otimes\frac{\mathbf{\Gamma}^\varepsilon}{n^\varepsilon}+\Pi^\varepsilon_\wedge\Big) + \frac{1}{\varepsilon}\nabla_\perp(n^\varepsilon T^\varepsilon) \tag{26b}$$
$$= \frac{1}{\varepsilon}\Big(-n^\varepsilon\nabla_\perp\phi^\varepsilon + \mathbf{\Gamma}^\varepsilon_\perp\times\mathbf{B}\Big),$$

where n^ε_0 stands for the initial density $n^\varepsilon(t=0)$.

Proof. The proof starts as in Proposition 1. Then insert into equation (22) the relation (23) and the identity

$$n^\varepsilon(t) = n^\varepsilon_0 + \int_0^t\frac{\partial n^\varepsilon(s)}{\partial s}\,ds, \tag{27}$$

where under the integrand we insert the mass conservation law (24) at time s.

Letting $\varepsilon\to 0$ in equation (26a) leads to

$$-\nabla_\parallel\Big[(T^0+T_e)\int_0^t\nabla_\parallel\Gamma^0_\parallel(s)\,ds\Big] - \nabla_\parallel\Big[(T^0+T_e)\int_0^t(\Gamma^0_\parallel\nabla\cdot\mathbf{b}+\nabla\cdot\mathbf{\Gamma}^0_\perp)(s)\,ds\Big]$$
$$= -\nabla_\parallel\Big[(T^0+T_e)n^0_0\Big]. \tag{28}$$

If the mass conservation law is satisfied we can use (27) to deduce $\nabla_\parallel[(T^0+T_e)n^0]=0$. Note that the zero force regime is recovered without any assumptions on the initial conditions, unlike the formulation of Proposition 1. □

3.2. **AP-formulation in a uniform B-field.** For the remainder of this work we assume a uniform $\mathbf{B}$-field in the z direction, $\mathbf{B}=\mathbf{b}=\mathbf{e}_z$. Moreover, we assume $\mathbf{x}=(x,y,z)\in\Omega$, with the finite spatial domain $\Omega=[0,L_x]\times[0,L_y]\times[0,L_z]$ and periodic boundary conditions in the z-direction. Now, the wave-like equation (21a) for the parallel flux reads

$$\varepsilon\frac{\partial^2\Gamma^\varepsilon_z}{\partial t^2} - \partial_z\Big[(T^\varepsilon+T_e)\partial_z\Gamma^\varepsilon_z\Big] - \partial_z\Big[(T^\varepsilon+T_e)\nabla\cdot\mathbf{\Gamma}^\varepsilon_\perp\Big]$$
$$+\partial_z\left[n^\varepsilon\frac{\partial(T^\varepsilon+T_e)}{\partial t}\right] = -\varepsilon\nabla\cdot\frac{\partial}{\partial t}\Big(\mathbf{\Gamma}^\varepsilon\frac{\Gamma^\varepsilon_z}{n^\varepsilon}\Big) - \varepsilon\Big(\nabla\cdot\frac{\partial}{\partial t}\Pi^\varepsilon_\wedge\Big)_z. \tag{29}$$

In the limit $\varepsilon\to 0$ we obtain the second order problem

$$-\partial_z\Big[(T^\varepsilon+T_e)\partial_z\Gamma^\varepsilon_z\Big] - \partial_z\Big[(T^\varepsilon+T_e)\nabla\cdot\mathbf{\Gamma}^\varepsilon_\perp\Big] + \partial_z\left[n^\varepsilon\frac{\partial(T^\varepsilon+T_e)}{\partial t}\right] = 0, \tag{30}$$

which is ill-posed due to the periodic boundary conditions. The limit equation (30) only accounts for the macroscopic part of the equation (29), associated to the dominant operator in the limit $\varepsilon \to 0$. Its solution is determined up to a function with a vanishing aligned gradient, which can be determined thanks to the microscopic information contained in (29). As mentioned in the introduction, there are multiple ways to restore the well posedness of the problem for $\varepsilon = 0$, operating a decomposition of the solution into a part in the kernel of the dominant operator defined by (30) complemented with a correction. The approach implemented here harnesses the duality-based decomposition [18] of Γ_z^ε into its mean and fluctuation along the z-direction. In what follows we denote the mean along z of a function $a(x, y, z)$ defined on Ω by

$$\overline{a}(x, y) := \frac{1}{L_z} \int_0^{L_z} a(x, y, z)\, dz\,, \tag{31}$$

The corresponding fluctuations are defined by

$$a' := a - \overline{a}\,, \qquad \Longrightarrow \qquad \overline{a'} = 0\,. \tag{32}$$

Hence, there exist two unique functions η^ε and ξ^ε satisfying

$$\Gamma_z^\varepsilon = \eta^\varepsilon + \xi^\varepsilon\,, \qquad \overline{\xi^\varepsilon} = 0\,. \tag{33}$$

Inserting the decomposition (33) into (29) and integrating with respect to z yields the equation for the mean,

$$\frac{\partial^2 \eta^\varepsilon}{\partial t^2} = -\nabla \cdot \frac{\partial}{\partial t}\Big(\overline{\mathbf{\Gamma}_\perp^\varepsilon \frac{\Gamma_z^\varepsilon}{n^\varepsilon}}\Big) - \Big(\overline{\nabla \cdot \frac{\partial}{\partial t} \Pi_\wedge^\varepsilon}\Big)_z\,. \tag{34}$$

This equation is coupled to (29), which is used to compute ξ^ε:

$$\begin{aligned} \varepsilon \frac{\partial^2 \xi^\varepsilon}{\partial t^2} + \varepsilon \frac{\partial^2 \eta^\varepsilon}{\partial t^2} - \partial_z \Big[(T^\varepsilon + T_e)\partial_z \xi^\varepsilon\Big] - \partial_z \Big[(T^\varepsilon + T_e)\nabla \cdot \mathbf{\Gamma}_\perp^\varepsilon\Big] \\ + \partial_z \left[n^\varepsilon \frac{\partial (T^\varepsilon + T_e)}{\partial t}\right] = -\varepsilon \nabla \cdot \frac{\partial}{\partial t}\Big(\mathbf{\Gamma}^\varepsilon \frac{\Gamma_z^\varepsilon}{n^\varepsilon}\Big) - \varepsilon \Big(\nabla \cdot \frac{\partial}{\partial t} \Pi_\wedge^\varepsilon\Big)_z\,, \end{aligned} \tag{35}$$

Remark that $\partial_z \eta^\varepsilon = 0$ by construction. In the limit $\varepsilon \to 0$ equation (35) degenerates to

$$-\partial_z \Big[(T^0 + T_e)\partial_z \xi^0\Big] - \partial_z \Big[(T^0 + T_e)\nabla \cdot \mathbf{\Gamma}_\perp^0\Big] + \partial_z \left[n^0 \frac{\partial (T^0 + T_e)}{\partial t}\right] = 0\,, \tag{36}$$

which is now a well-posed problem for ξ^0 due to the integral constraint $\overline{\xi^0} = 0$. We see that the duality-based AP reformulation based on (33) requires integration along the magnetic field lines. This is easily done for straight field lines but remains challenging for field lines that do not coincide with the space mesh. Different techniques exist for the latter case, which we aim to employ in a forthcoming work.

For clarity, let us summarize here the obtained problem reformulation, based on the wave equation for $\Gamma_z^\varepsilon = \eta^\varepsilon + \xi^\varepsilon$. We will work with an equation for the temperature T^ε instead of the energy w^ε (the conservative form of the fluid equations is not paramount for

our scheme and more generally for plasma under large magnetic fields). The (AP)-model corresponding to the (EL)-system (1) reads

$$(AP)\begin{cases} \dfrac{\partial n^\varepsilon}{\partial t} + \partial_z \Gamma_z^\varepsilon + \nabla\cdot \mathbf{\Gamma}_\perp^\varepsilon = 0\,, \qquad \Gamma_z^\varepsilon = \eta^\varepsilon + \xi^\varepsilon\,, \qquad \overline{\xi^\varepsilon} = 0\,, \\ \dfrac{\partial^2 \eta^\varepsilon}{\partial t^2} = -\nabla\cdot \dfrac{\partial}{\partial t}\Big(\overline{\mathbf{\Gamma}^\varepsilon \dfrac{\Gamma_z^\varepsilon}{n^\varepsilon}}\Big) - \Big(\overline{\nabla\cdot \dfrac{\partial}{\partial t}\Pi_\wedge^\varepsilon}\Big)_z\,, \\ \varepsilon \dfrac{\partial^2 \xi^\varepsilon}{\partial t^2} + \varepsilon \dfrac{\partial^2 \eta^\varepsilon}{\partial t^2} - \partial_z\Big[(T^\varepsilon + T_e)\partial_z \xi^\varepsilon\Big] - \partial_z\Big[(T^\varepsilon + T_e)\nabla\cdot \mathbf{\Gamma}_\perp^\varepsilon\Big] \\ \qquad + \partial_z\left[n^\varepsilon \dfrac{\partial (T^\varepsilon + T_e)}{\partial t}\right] = -\varepsilon \nabla\cdot \dfrac{\partial}{\partial t}\Big(\mathbf{\Gamma}^\varepsilon \dfrac{\Gamma_z^\varepsilon}{n^\varepsilon}\Big) - \varepsilon\Big(\nabla\cdot \dfrac{\partial}{\partial t}\Pi_\wedge^\varepsilon\Big)_z\,, \\ \dfrac{\partial \mathbf{\Gamma}_\perp^\varepsilon}{\partial t} + \nabla\cdot\Big(\mathbf{\Gamma}^\varepsilon \otimes \dfrac{\mathbf{\Gamma}_\perp^\varepsilon}{n^\varepsilon} + \Pi_{\wedge,\perp}^\varepsilon\Big) + \dfrac{1}{\varepsilon}\nabla_\perp (n^\varepsilon T^\varepsilon) = \dfrac{1}{\varepsilon}\Big(- n^\varepsilon \nabla_\perp \phi^\varepsilon + \mathbf{\Gamma}_\perp^\varepsilon \times \mathbf{e}_z\Big)\,, \\ \dfrac{\partial T^\varepsilon}{\partial t} + \nabla\cdot\Big(\dfrac{\mathbf{\Gamma}^\varepsilon}{n^\varepsilon} T^\varepsilon\Big) - \dfrac{1}{3} T^\varepsilon \nabla\cdot\Big(\dfrac{\mathbf{\Gamma}^\varepsilon}{n^\varepsilon}\Big) + \dfrac{2}{3}\dfrac{1}{n^\varepsilon}\nabla\cdot \mathbf{q}_\wedge^\varepsilon = 0\,, \\ \phi^\varepsilon = T_e \ln\Big(\dfrac{n^\varepsilon}{n_c}\Big)\,. \end{cases} \tag{37}$$

The system (37) is defined on $[0,\mathcal{T}]\times\Omega \subset \mathbb{R}^3$, where $\mathcal{T} > 0$ and Ω is a rectangular parallelepiped $\Omega = [0, L_x]\times[0,L_y]\times[0,L_z]$. It is supplemented with initial conditions,

$$n^\varepsilon(t=0,\mathbf{x}) = n_0^\varepsilon(\mathbf{x})\,, \qquad \mathbf{\Gamma}^\varepsilon(t=0,\mathbf{x}) = \mathbf{\Gamma}_0^\varepsilon(\mathbf{x})\,, \qquad T^\varepsilon(t=0,\mathbf{x}) = T_0^\varepsilon(\mathbf{x})\,, \tag{38}$$

$$\varepsilon \frac{\partial \Gamma_z^\varepsilon}{\partial t}\Big|_{t=0} + \varepsilon \nabla\cdot\left(\mathbf{\Gamma}_0^\varepsilon \frac{\Gamma_{z,0}^\varepsilon}{n_0^\varepsilon}\right) + \partial_z[(T_0^\varepsilon + T_e) n_0^\varepsilon]) + \varepsilon(\nabla\cdot \Pi_{\wedge,0}^\varepsilon)_z = 0\,, \tag{39}$$

$$\eta^\varepsilon(t=0,x,y) = \frac{1}{L_z}\int_0^{L_z} \Gamma_{z,0}^\varepsilon\, dz\,, \qquad \xi^\varepsilon(t=0,\mathbf{x}) = \Gamma_{z,0}^\varepsilon - \eta^\varepsilon(t=0,x,y)\,, \tag{40}$$

and boundary conditions,

$$\begin{cases} \text{Dirichlet:} \quad n^\varepsilon(t,0,y,z) = n_l\,, \qquad n^\varepsilon(t,L_x,y,z) = n_r\,, \\ \qquad\qquad\quad T^\varepsilon(t,0,y,z) = T_l\,, \qquad T^\varepsilon(t,L_x,y,z) = T_r\,, \\ \text{Neumann:} \quad \partial_x \mathbf{\Gamma}^\varepsilon(t,0,y,z) = \partial_x \mathbf{\Gamma}^\varepsilon(t,L_x,y,z) = 0\,, \\ \qquad\qquad\quad \partial_x \eta^\varepsilon(t,0,y,z) = \partial_x \eta^\varepsilon(t,L_x,y,z) = 0\,, \\ \qquad\qquad\quad \partial_x \xi^\varepsilon(t,0,y,z) = \partial_x \xi^\varepsilon(t,L_x,y,z) = 0\,, \\ + \text{periodic boundary conditions in } y \text{ and } z. \end{cases} \tag{41}$$

Here, n_l, n_r, T_l and T_r are fixed constant densities and temperatures at the x-boundaries, respectively.

4. Drift-asymptotic numerical scheme

We shall now write the asymptotic-preserving numerical scheme for the (EL)-system (1). The scheme is based on the ideas elaborated in the previous section, in particular on the reformulation of the conservation law for Γ_z^ε, in a uniform magnetic field $\mathbf{B} = \mathbf{e}_z$. This reformulation is carried out here on the time semi-discrete level, which is simpler than discretizing the (AP)-model (37) directly. After semi-discretization in time, in a second step the spatial discretization is presented. We implement a finite volume scheme for hyperbolic conservations laws [39], with an artificial viscosity of local Lax-Friedrichs (Rusanov) form. A von Neumann stability analysis brings some insight into the CFL-condition on the time step in our scheme.

4.1. **Semi-discretization in time.** In what follows we omit the superscript ε on the unknowns for the sake of a more transparent notation. For a function $a(t)$ defined on $\mathbb{R}^+$ we denote

$$a^m = a(t^m)\,, \qquad t^m = \sum_{q=0}^{m} (\Delta t)_{q-1}\,, \qquad (\Delta t)_{-1} = 0\,, \tag{42}$$

where $(\Delta t)_q$ is a variable time step, defined later via a CFL-condition. For more transparency in the notation we set $(\Delta t)_q \equiv \Delta t$ in what follows, even though variable time stepping is allowed in the simulations. The starting point is a time semi-discretization, where the implicitness of the parallel mass flux, the parallel pressure gradient as well as the momentum in the Lorentz force are mandatory:

$$(EL)_{\Delta t} \begin{cases} \dfrac{n^{m+1}-n^m}{\Delta t} + \partial_z \Gamma_z^{m+1} + \nabla\cdot\boldsymbol{\Gamma}_\perp^{m+1} = 0\,, \\ \dfrac{\Gamma_z^{m+1}-\Gamma_z^m}{\Delta t} + \nabla\cdot\Big(\boldsymbol{\Gamma}^{m/m+1}\otimes\dfrac{\Gamma_z^m}{n^m}\Big) + \dfrac{1}{\varepsilon}\partial_z[(T^m+T_e)n^{m+1}] + (\nabla\cdot\Pi_\wedge^m)_z = 0\,, \\ \dfrac{\boldsymbol{\Gamma}_\perp^{m+1}-\boldsymbol{\Gamma}_\perp^m}{\Delta t} + \nabla\cdot\Big(\boldsymbol{\Gamma}^m\otimes\dfrac{\boldsymbol{\Gamma}_\perp^m}{n^m} + \Pi_{\wedge,\perp}^m\Big) + \dfrac{1}{\varepsilon}\nabla_\perp(n^mT^m) \\ \qquad\qquad = \dfrac{1}{\varepsilon}\Big(-n^m\nabla_\perp\phi^m + \boldsymbol{\Gamma}_\perp^{m+1}\times\mathbf{e}_z\Big)\,, \\ \dfrac{T^{m+1}-T^m}{\Delta t} + \nabla\cdot\Big(\dfrac{\boldsymbol{\Gamma}^{m+1}}{n^m}T^m\Big) - \dfrac{1}{3}T^m\nabla\cdot\Big(\dfrac{\boldsymbol{\Gamma}^{m+1}}{n^m}\Big) + \dfrac{2}{3}\dfrac{1}{n^m}\nabla\cdot\mathbf{q}_\wedge^m = 0\,, \\ \phi^{m+1} = T_e\ln\Big(\dfrac{n^{m+1}}{n_c}\Big)\,, \end{cases} \tag{43}$$

where $\boldsymbol{\Gamma}^{m/m+1} = (\boldsymbol{\Gamma}_\perp^{m+1}, \Gamma_z^m)$ but this quantity could have been left totally explicit, as well as the momentum in the temperature equation. However the resolution of the equations can be sequenced is such a way that these implicitations come at no cost. Note that we used relation (23) in the second equation and that the last equation furnishes an initial condition for the electric potential ϕ^0. Inserting now the density n^{m+1} from the first equation into the

pressure term of the second equation, multiplying by ε, applying the unique decomposition (33) for the parallel flux, i.e. $\Gamma_z^{m+1} = \eta^{m+1} + \xi^{m+1}$ with $\overline{\xi^{m+1}} = 0$ and $\partial_z \eta^{m+1} = 0$, we obtain the semi discrete AP-scheme

$$(AP)_{\Delta t} \begin{cases} \dfrac{n^{m+1}-n^m}{\Delta t} + \partial_z \Gamma_z^{m+1} + \nabla \cdot \mathbf{\Gamma}_\perp^{m+1} = 0\,, \quad \Gamma_z^{m+1} = \eta^{m+1} + \xi^{m+1}\,, \quad \overline{\xi^{m+1}} = 0\,, \\ \dfrac{\eta^{m+1}-\eta^m}{\Delta t} + \nabla \cdot \Big(\overline{\mathbf{\Gamma}_\perp^{m+1} \otimes \dfrac{\Gamma_z^m}{n^m}} \Big) + (\overline{\nabla \cdot \Pi_\wedge^m})_z = 0\,, \\ \dfrac{\varepsilon}{\Delta t}(\xi^{m+1} + \eta^{m+1} - \Gamma_z^m) + \varepsilon \nabla \cdot \Big(\mathbf{\Gamma}^{m/m+1} \otimes \dfrac{\Gamma_z^m}{n^m} \Big) - \Delta t \partial_z [(T^m + T_e)\partial_z \xi^{m+1}] \\ \qquad\qquad + \partial_z [(T^m + T_e) n^m] - \Delta t \partial_z [(T^m + T_e) \nabla \cdot \mathbf{\Gamma}_\perp^{m+1}] + \varepsilon (\nabla \cdot \Pi_\wedge^m)_z = 0\,, \\ \dfrac{\mathbf{\Gamma}_\perp^{m+1} - \mathbf{\Gamma}_\perp^m}{\Delta t} + \nabla \cdot \Big(\mathbf{\Gamma}^m \otimes \dfrac{\mathbf{\Gamma}_\perp^m}{n^m} + \Pi_{\wedge,\perp}^m \Big) + \dfrac{1}{\varepsilon} \nabla_\perp (n^m T^m) \\ \qquad\qquad = \dfrac{1}{\varepsilon} \Big(- n^m \nabla_\perp \phi^m + \mathbf{\Gamma}_\perp^{m+1} \times \mathbf{e}_z \Big)\,, \\ \dfrac{T^{m+1}-T^m}{\Delta t} + \nabla \cdot \Big(\dfrac{\mathbf{\Gamma}^{m+1}}{n^m} T^m \Big) - \dfrac{1}{3} T^m \nabla \cdot \Big(\dfrac{\mathbf{\Gamma}^{m+1}}{n^m} \Big) + \dfrac{2}{3} \dfrac{1}{n^m} \nabla \cdot \mathbf{q}_\wedge^m = 0\,, \\ \phi^{m+1} = T_e \ln \Big(\dfrac{n^{m+1}}{n_c} \Big)\,, \end{cases} \tag{44}$$

The cycle for solving the system (44) at each instant t^m is as follows:

$$\text{start loop:} \quad \mathbf{\Gamma}_\perp^{m+1} \to \eta^{m+1} \to \xi^{m+1} \to (n^{m+1}, T^{m+1}) \to \phi^{m+1} \quad \text{end of loop.}$$

Some of the individual steps in the loop require a more detailed discussion:

- Computation of $\mathbf{\Gamma}_\perp^{m+1}$: For $\varepsilon \geq 0$ and for a general magnetic field $\mathbf{B}$, the simple case $\mathbf{B} = \mathbf{e}_z$ included, we introduce the matrix $\Omega_\mathbf{B}$, defined via $\Omega_\mathbf{B}(\cdot) := (\cdot) \times \mathbf{B}$. The matrix reads

$$\Omega_\mathbf{B} = \begin{pmatrix} 0 & B_z & -B_y \\ -B_z & 0 & B_x \\ B_y & -B_x & 0 \end{pmatrix}. \tag{45}$$

We further introduce the parameter $\kappa := \varepsilon / \Delta t$. For $\kappa > 0$ the matrix $\kappa \mathbb{I}\mathrm{d} - \Omega_\mathbf{B}$ is invertible, $\mathbb{I}\mathrm{d}$ denoting the identity matrix,

$$\Big(\kappa \mathbb{I}\mathrm{d} - \Omega_\mathbf{B} \Big)^{-1} = \frac{1}{\kappa(|\mathbf{B}|^2 + \kappa^2)} \left[\kappa^2 \mathbb{I}\mathrm{d} + \kappa \Omega_\mathbf{B} + (\mathbf{B} \otimes \mathbf{B}) \right]. \tag{46}$$

This last expression emphasizes the singularity of the matrix $\kappa \mathbb{I}\mathrm{d} - \Omega_\mathbf{B}$ in the limit $\kappa \to 0$. However, the matrix $[\kappa \mathbb{I}\mathrm{d} - \Omega_\mathbf{B}]$ is invertible on the orthogonal of the $\mathbf{b} \otimes \mathbf{b}$-operator kernel for all values $\kappa \geq 0$. The projector on this kernel orthogonal reads $\mathbb{I}\mathrm{d} - \mathbf{b} \otimes \mathbf{b}$, which is the projector on the local perpendicular plane with respect to $\mathbf{B}$. Hence we define the matrix

Θ_κ, invertible for $\kappa \geq 0$,

$$\Theta_\kappa := (\kappa \mathbb{I}\mathrm{d} - \Omega_{\mathbf{B}})^{-1}(\mathbb{I}\mathrm{d} - \mathbf{b}\otimes\mathbf{b}) = \frac{1}{|\mathbf{B}|^2+\kappa^2}\left[\kappa(\mathbb{I}\mathrm{d} - \mathbf{b}\otimes\mathbf{b}) + \Omega_{\mathbf{B}}\right]. \tag{47}$$

With the help of this matrix, the perpendicular flux in system (44) is obtained as

$$\mathbf{\Gamma}_\perp^{m+1} = \Theta_\kappa^m \left[\kappa \mathbf{\Gamma}_\perp^m - \varepsilon\nabla\cdot\left(\mathbf{\Gamma}^m \otimes \frac{\mathbf{\Gamma}_\perp^m}{n^m} + \Pi_{\wedge,\perp}^m\right) - \nabla_\perp(n^m T^m) - n^m\nabla_\perp\phi^m\right]. \tag{48}$$

Equation (48) is an expansion of the perpendicular flux at time t^{m+1} in powers of ε around the drift approximation $\mathbf{\Gamma}_D^m$, defined as

$$\mathbf{\Gamma}_D^m := -n^m\nabla_\perp\phi^m \times \mathbf{e}_z - \nabla_\perp(n^m T^m)\times\mathbf{e}_z\,. \tag{49}$$

Indeed, the drift approximation appears as the zero-order term in (48).

- Computation of ξ^{m+1}: the equation for the fluctuation ξ^{m+1} of the parallel flux is a one-dimensional heat equation in the parallel direction, with the constraint of zero mean on the solution. The coordinates (x, y) appear only as parameters. This can be a strong point of our scheme when thinking of parallelization. The constraint can be implemented by introducing a Lagrange multiplier $\lambda^{m+1}(x, y)$, independent of z. In particular, we solve

$$\begin{aligned}\frac{\varepsilon}{\Delta t}\xi^{m+1} - \Delta t\partial_z[(T^m+T_e)\partial_z\xi^{m+1}] + \lambda^{m+1} = -\frac{\varepsilon}{\Delta t}(\eta^{m+1}-\Gamma_z^m) - \varepsilon\nabla\cdot\left(\mathbf{\Gamma}^{m/m+1}\otimes\frac{\Gamma_z^m}{n^m}\right)\\ - \partial_z[(T^m+T_e)n^m] + \Delta t\partial_z[(T^m+T_e)\nabla\cdot\mathbf{\Gamma}_\perp^{m+1}] - \varepsilon(\nabla\cdot\Pi_\wedge^m)_z\,,\end{aligned} \tag{50}$$

$\overline{\xi^{m+1}} = 0\,.$

The Lagrange multiplier is an additional unknown which supplements the equation for the constraint. Integrating equation (50) along z yields $\lambda^{m+1}\equiv 0$.

4.2. **Cancellation of the diamagnetic drift.** The gyro-viscous stress tensor $\Pi_\wedge^\varepsilon$ and heat flux $\mathbf{q}_\wedge^\varepsilon$ were included in the (EL)-model (1) for the sake of the correct description of the low frequency physics in the drift regime $\varepsilon \ll 1$, in particular of the ion-temperature-gradient (ITG) modes. In order to simplify the implementation of the numerical scheme, we take into account only those gyro-viscous terms necessary for the correct ITG dispersion relation, which is given in (90). Hence, we define

$$\Pi_\wedge^\varepsilon := \frac{n^\varepsilon T^\varepsilon}{2}\begin{pmatrix}0&0&-2\partial_y u_z^\varepsilon\\0&0&2\partial_x u_z^\varepsilon\\0&0&0\end{pmatrix}, \qquad \mathbf{q}_\wedge^\varepsilon := -\frac{5}{2}n^\varepsilon T^\varepsilon\begin{pmatrix}-\partial_y T^\varepsilon\\ \partial_x T^\varepsilon\\0\end{pmatrix}, \tag{51}$$

which leads to

$$(\nabla\cdot\Pi_\wedge^\varepsilon)_\perp = 0\,, \qquad (\nabla\cdot\Pi_\wedge^\varepsilon)_z = -\left\{n^\varepsilon T^\varepsilon, \frac{\Gamma_z^\varepsilon}{n^\varepsilon}\right\}, \qquad \nabla\cdot\mathbf{q}_\wedge^\varepsilon = -\frac{5}{2}\left\{n^\varepsilon T^\varepsilon, T^\varepsilon\right\}, \tag{52}$$

where $\{\mu,\nu\} = \partial_x\mu\partial_y\nu - \partial_y\mu\partial_x\nu$ stands for the Poisson bracket in the xy-plane. Employing the relations (52) we shall explicitly account for the cancellation of the diamagnetic drift

terms in our numerical scheme. Using the drift approximation (49), remark thus the identities

$$\nabla \cdot \mathbf{\Gamma}_D^m = \{\phi^m, n^m\}\,, \qquad \mathbf{\Gamma}_D^m \cdot \nabla(\cdot) = n^m\{\phi^m, \cdot\} + \{n^m T^m, \cdot\}\,. \tag{53}$$

We now use (52) and (53) to rewrite the semi-discrete system (43). For some number $\sigma \geq 0$, we rewrite the particle conservation law as

$$\frac{n^{m+1} - n^m}{\Delta t} + \partial_z \Gamma_z^{m+1} + \nabla \cdot [\mathbf{\Gamma}_\perp^{m+1} - \sigma \mathbf{\Gamma}_D^m] + \sigma\{\phi^m, n^m\} = 0\,, \tag{54a}$$

the parallel momentum conservation law as

$$\frac{\Gamma_z^{m+1} - \Gamma_z^m}{\Delta t} + \nabla \cdot \Big[(\mathbf{\Gamma}^{m/m+1} - \sigma \mathbf{\Gamma}_D^m) \otimes \frac{\Gamma_z^m}{n^m}\Big] + \frac{1}{\varepsilon}\partial_z[(T^m + T_e)n^{m+1}] \tag{54b}$$

$$+ \sigma\{\phi^m, \Gamma_z^m\} + (\sigma - 1)\Big\{n^m T^m, \frac{\Gamma_z^m}{n^m}\Big\} = 0\,, \tag{54c}$$

and, finally, the temperature equation as

$$\begin{aligned} &\frac{T^{m+1} - T^m}{\Delta t} + \nabla \cdot \Big[(\mathbf{\Gamma}^{m+1} - \sigma \mathbf{\Gamma}_D^m)\frac{T^m}{n^m}\Big] - \frac{1}{3}T^m \nabla \cdot \Big[\frac{(\mathbf{\Gamma}^{m+1} - \sigma \mathbf{\Gamma}_D^m)}{n^m}\Big] \\ &\qquad + \sigma\{\phi^m, T^m\} + (\sigma - 1)\frac{5}{3}\frac{T^m}{n^m}\{n^m, T^m\} = 0\,. \end{aligned} \tag{54d}$$

In what follows, $\sigma : \mathbb{R}^+ \to [0, 1]$ will be some function with the properties

$$\sigma(0) = 1\,, \qquad \sigma(\varepsilon) = 0 \quad \text{for} \quad \varepsilon \geq 1\,, \qquad \frac{\sigma(\varepsilon_1) - \sigma(\varepsilon_2)}{\varepsilon_1 - \varepsilon_2} \leq 0 \quad \text{for} \quad \varepsilon_1 \neq \varepsilon_2\,. \tag{55}$$

This function will serve as an ε-dependent switch, choosing between different formulations in the regimes $\varepsilon \sim 1$ and $\varepsilon \to 0$, respectively. For $\varepsilon \geq 1$ one obtains the original formulation (43). In the case $\varepsilon = 0$, however, we have $\sigma = 1$ and $\mathbf{\Gamma}_\perp^{m+1} = \mathbf{\Gamma}_D^m$, such that the equations (54) read

$$\frac{n^{m+1} - n^m}{\Delta t} + \partial_z \Gamma_z^{m+1} + \{\phi^m, n^m\} = 0\,, \tag{56a}$$

$$\frac{\Gamma_z^{m+1} - \Gamma_z^m}{\Delta t} + \partial_z\Big[\frac{(\Gamma_z^m)^2}{n^m}\Big] + \frac{1}{\varepsilon}\partial_z[(T^m + T_e)n^{m+1}] + \{\phi^m, \Gamma_z^m\} = 0\,, \tag{56b}$$

$$\frac{T^{m+1} - T^m}{\Delta t} + \partial_z\Big(\Gamma_z^{m+1}\frac{T^m}{n^m}\Big) - \frac{1}{3}T^m\partial_z\Big(\frac{\Gamma_z^{m+1}}{n^m}\Big) + \{\phi^m, T^m\} = 0\,. \tag{56c}$$

Note that the diamagnetic drift is absent in the Poisson brackets, a consequence of the the vanishing Larmor-radius as $\varepsilon \to 0$. To lowest order, finite Larmor radius effects do not contribute to the macroscopic plasma drift, fact which is guarantueed by the gyro-viscous Braginskii terms (51). Note that the above manipulations on the system (43) carry over to the AP-system (44). In our code we implemented a function σ that depends on γ^ε, which

is an indicator of the regime investigated, defined as the ratio of the small scale ε to the squared mesh size (see equation (78)):

$$\sigma = \begin{cases} 0 & \text{if} \quad \gamma^\varepsilon > 1\,, \\ 1 & \text{if} \quad \gamma^\varepsilon \leq 1\,. \end{cases} \tag{57}$$

Remark 2. *The rewriting of the scheme in the form* (54) *and the introduction of the switch function σ are not related to the asymptotic preserving properties of the scheme but to that of the conservation of specific equilibrium states. This feature will be discussed in more detail for the ITG simulation. The definition* (57) *of the switch function σ is quite coarse, with a non smooth transition from one formulation to another. Particular attention should be paid to this definition in future work.*

4.3. **Space discretization.** We implement a local Lax-Friedrichs (Rusanov) scheme [39] for the space discretization of the system (44). The mesh covering the spatial domain $\Omega = [0, L_x] \times [0, L_y] \times [0, L_z]$ is the following:

$$\begin{gathered} x_i = (i-1)\Delta x\,, \qquad y_j = (j-1)\Delta y\,, \qquad z_k = (k-1)\Delta z\,, \\ \Delta x = \frac{L_x}{N_x - 1}\,, \qquad \Delta y = \frac{L_y}{N_y - 1}\,, \qquad \Delta z = \frac{L_z}{N_z - 1}\,, \end{gathered} \tag{58}$$

where

$$i \in \{1, \ldots, N_x\}\,, \qquad j \in \{1, \ldots, N_y - 1\}\,, \qquad k \in \{1, \ldots, N_z - 1\}\,. \tag{59}$$

A function μ defined on Ω is approximated by its values at the nodes, $\mu_{i,j,k} = \mu(x_i, y_j, z_k)$. Due to the periodicity in the y- and in the z-direction one has

$$\mu_{i,N_y,k} = \mu_{i,1,k} \quad \forall\, i,k \qquad \text{and} \qquad \mu_{i,j,N_z} = \mu_{i,j,1} \quad \forall\, i,j\,. \tag{60}$$

To implement the Neumann boundary conditions (also called non-reflecting) in the x-direction we install ghost points with the indices $i = 0$ and $i = N_x + 1$, repsectively, and set

$$\mathbf{\Gamma}^m_{0,j,k} = \mathbf{\Gamma}^m_{1,j,k} \qquad \text{and} \qquad \mathbf{\Gamma}^m_{N_{x+1},j,k} = \mathbf{\Gamma}^m_{N_x,j,k} \qquad \forall\, j,k,m\,. \tag{61}$$

Space differentials are approximated by standard centered finite differences. In the Rusanov scheme, for each unknown μ^m one defines an artificial numerical flux $\mathcal{Q}^m_\mu \in \mathbb{R}^3$ at time $m\Delta t$. The components of the numerical flux in the different space direction are denoted by $\mathcal{Q}^m_\mu = (\mathcal{X}^m_\mu, \mathcal{Y}^m_\mu, \mathcal{Z}^m_\mu)$. They are defined at the half-points, i.e. between the nodes defined in (58). The artificial fluxes $\mathcal{Q}^m_\mu$ will guarantuee the stability of the scheme, and are defined as

$$\begin{aligned} \mathcal{X}^m_{\mu,i+1/2} &= -\frac{a^m_{i+1/2}}{2}(\mu^m_{i+1} - \mu^m_i)\,, \\ \mathcal{Y}^m_{\mu,j+1/2} &= -\frac{a^m_{j+1/2}}{2}(\mu^m_{j+1} - \mu^m_j)\,, \\ \mathcal{Z}^m_{\mu,k+1/2} &= -\frac{a^m_{k+1/2}}{2}(\mu^m_{k+1} - \mu^m_k)\,, \end{aligned} \tag{62}$$

for each unknown μ. Remark that, whenever a spatial index is not stated explicitly, it is i, j or k, respectively. The local viscosities in (62) are determined from

$$\begin{aligned} a^m_{i+1/2} &= \max\left(\left|\frac{\Gamma^m_x}{n^m}\right|, \left|\frac{\Gamma^m_{x,i+1}}{n^m}\right|\right) + \sqrt{\max_\Omega(T^m + T_e)}\,, \\ a^m_{j+1/2} &= \max\left(\left|\frac{\Gamma^m_y}{n^m}\right|, \left|\frac{\Gamma^m_{y,j+1}}{n^m}\right|\right) + \sqrt{\max_\Omega(T^m + T_e)}\,, \\ a^m_{k+1/2} &= \max\left(\left|\frac{\Gamma^m_z}{n^m}\right|, \left|\frac{\Gamma^m_{z,k+1}}{n^m}\right|\right) + \sqrt{\max_\Omega(T^m + T_e)}\,, \end{aligned} \tag{63}$$

Note that we do not take a local but the global maximum of the temperature in these relations; this stems from the fact that we want our scheme to conserve equilibria with non-vanishing temperature gradients. Artificial viscosities $a^m = a^m(x)$ would destroy such a property. We remark also that the Rusanov scheme has usually less artificial viscosity than the Lax-Friedrichs scheme, which is obtained for $a^m_{i+1/2} = \Delta x/\Delta t$, $a^m_{j+1/2} = \Delta y/\Delta t$ and $a^m_{k+1/2} = \Delta z/\Delta t$.

Poisson brackets are discretized with the Arakawa scheme [1]. The discrete version of the bracket $\{\mu, \nu\}$ evaluated at the point (x_i, y_j) is defined as

$$\begin{aligned} \{\mu,\nu\}_{ij} := \frac{1}{12\Delta x\Delta y}\Big(&\mu_{i+1j}\mathcal{A}_{ij} + \mu_{i-1j}\mathcal{B}_{ij} + \mu_{ij+1}\mathcal{C}_{ij} + \mu_{ij-1}\mathcal{D}_{ij} \\ &+\mu_{i+1j+1}\mathcal{E}_{ij} + \mu_{i-1j-1}\mathcal{F}_{ij} + \mu_{i-1j+1}\mathcal{G}_{ij} + \mu_{i+1j-1}\mathcal{H}_{ij}\Big)\,, \end{aligned} \tag{64}$$

where the coefficients read

$$\begin{aligned} \mathcal{A}_{ij} &:= +\nu_{ij+1} - \nu_{ij-1} + \nu_{i+1j+1} - \nu_{i+1j-1}\,, & \mathcal{E}_{ij} &:= +\nu_{ij+1} - \nu_{i+1j}\,, \\ \mathcal{B}_{ij} &:= -\nu_{ij+1} + \nu_{ij-1} - \nu_{i-1j+1} + \nu_{i-1j-1}\,, & \mathcal{F}_{ij} &:= -\nu_{i-1j} + \nu_{ij-1}\,, \\ \mathcal{C}_{ij} &:= -\nu_{i+1j} + \nu_{i-1j} - \nu_{i+1j+1} + \nu_{i-1j+1}\,, & \mathcal{G}_{ij} &:= -\nu_{ij+1} + \nu_{i-1j}\,, \\ \mathcal{D}_{ij} &:= +\nu_{i+1j} - \nu_{i-1j} + \nu_{i+1j-1} - \nu_{i-1j-1}\,, & \mathcal{H}_{ij} &:= +\nu_{i+1j} - \nu_{ij-1}\,. \end{aligned} \tag{65}$$

4.4. **The CFL-condition.** In the Rusanov scheme the artificial fluxes (62) provide the numerical diffusion leading to stability. For this, the time step $(\Delta t)_m$ at time t^m must satisfy

$$(\Delta t)_m < \frac{1}{\max_i(a^m_{i+1/2})/\Delta x + \max_j(a^m_{j+1/2})/\Delta y + \max_k(a^m_{k+1/2})/\Delta z}\,. \tag{66}$$

Note that the time steps computed in this way do not depend[1] on ε, fact which stems from discretizing stiff terms in (44) implicitly. Unfortunately, our numerical tests revealed that the condition (66) is not sufficient for stability in all ε-regimes. Indeed, we shall show that there is a more restrictive CFL-condition in an intermediate ε-regime, i.e. when ε is of the order of $(\Delta x)^2$ or $(\Delta y)^2$, respectively, the square of the mesh parameters in the

[1]They depend implicitly on ε via the unknowns $\mathbf{\Gamma}^m$, n^m and T^m.

perpendicular plane (to $\mathbf{B}$). The situation is best explained by means of the following toy model ($\mathbf{B} = \mathbf{e}_z$):

$$\begin{cases} \dfrac{n^{m+1} - n^m}{\Delta t} + \nabla \cdot \mathbf{\Gamma}_\perp^m = 0\,, \\ \dfrac{\mathbf{\Gamma}_\perp^{m+1} - \mathbf{\Gamma}_\perp^m}{\Delta t} + \dfrac{1}{\varepsilon}\nabla_\perp n^m = \dfrac{1}{\varepsilon}\mathbf{\Gamma}_\perp^{m+1} \times \mathbf{e}_z\,. \end{cases} \tag{67}$$

This simple model corresponds to the discretization of the rotation term ($\mathbf{B}$-field term) in (44). We analyze the numerical stability of a standard Lax-Friedrichs scheme for (67):

$$\begin{cases} n_{\alpha,\beta}^{m+1} = \dfrac{1}{4}(n_{\alpha+1,\beta}^m + n_{\alpha-1,\beta}^m + n_{\alpha,\beta+1}^m + n_{\alpha,\beta-1}^m) \\ \qquad\qquad - \dfrac{\Delta t}{2\Delta x}(\Gamma_{x,\alpha+1,\beta}^m - \Gamma_{x,\alpha-1,\beta}^m) - \dfrac{\Delta t}{2\Delta y}(\Gamma_{y,\alpha,\beta+1}^m - \Gamma_{y,\alpha,\beta-1}^m)\,, \\ \dfrac{\varepsilon}{\Delta t}\Gamma_{x,\alpha,\beta}^{m+1} - \Gamma_{y,\alpha,\beta}^{m+1} = \dfrac{\varepsilon}{4\Delta t}(\Gamma_{x,\alpha+1,\beta}^m + \Gamma_{x,\alpha-1,\beta}^m + \Gamma_{x,\alpha,\beta+1}^m + \Gamma_{x,\alpha,\beta-1}^m) \\ \qquad\qquad - \dfrac{1}{2\Delta x}(n_{\alpha+1,\beta}^m - n_{\alpha-1,\beta}^m)\,, \\ \dfrac{\varepsilon}{\Delta t}\Gamma_{y,\alpha,\beta}^{m+1} + \Gamma_{x,\alpha,\beta}^{m+1} = \dfrac{\varepsilon}{4\Delta t}(\Gamma_{y,\alpha+1,\beta}^m + \Gamma_{y,\alpha-1,\beta}^m + \Gamma_{y,\alpha,\beta+1}^m + \Gamma_{y,\alpha,\beta-1}^m) \\ \qquad\qquad - \dfrac{1}{2\Delta y}(n_{\alpha,\beta+1}^m - n_{\alpha,\beta-1}^m)\,. \end{cases} \tag{68}$$

Defining $U^m := (n^m, \Gamma_x^m, \Gamma_y^m)$ the system (68) may be written as $U^{m+1} = AU^m$ with matrix A. A stability criterion in the L^2-norm can be obtained with the von Neumann method; a scheme is said to be stable if there exists a constant $0 < \nu < 1$ such that

$$||U^{m+1}||_2 \leq \nu ||U^m||_2\,, \tag{69}$$

where the discrete L^2-norm is defined as

$$||U^m||_2 := \left[\Delta x \Delta y \sum_\alpha \sum_\beta (|n_{\alpha,\beta}^m|^2 + |\Gamma_{x,\alpha,\beta}^m|^2 + |\Gamma_{y,\alpha,\beta}^m|^2)\right]^{1/2}. \tag{70}$$

Inserting into (68) the grid wave functions

$$n_{\alpha,\beta}^m = e^{i(\alpha\Delta x)\xi}\, e^{i(\beta\Delta y)\eta}\,, \qquad \Gamma_{x,\alpha,\beta}^m = e^{i(\alpha\Delta x)\xi}\, e^{i(\beta\Delta y)\eta}\,, \qquad \Gamma_{y,\alpha,\beta}^m = e^{i(\alpha\Delta x)\xi}\, e^{i(\beta\Delta y)\eta}\,, \tag{71}$$

we obtain a system $U^{m+1} = A(\xi,\eta)U^m$. The three eigenvalues of the matrix $A(\xi,\eta)$ are denoted by $\lambda_k(\xi,\eta)$ with $k \in \{1,2,3\}$; they are called the amplification coefficients of the respective eigenvector. The scheme is stable if $|\lambda_k(\xi,\eta)| \leq \nu$ for all $(\xi,\eta) \in \mathbb{R}^2$ and all k. Otherwise, there may be Fourier components that grow during time iteration.

It is easily shown that if one takes an explicit rotation term in (67), i.e. $\mathbf{\Gamma}^m_\perp \times \mathbf{e}_z$, the von Neumann analysis yields the CFL-condition

$$\Delta t < \frac{1}{\sqrt{2}} \min\left(\sqrt{\varepsilon}\Delta x, \sqrt{\varepsilon}\Delta y, \varepsilon\right) . \tag{72}$$

In this case the time step is severely restricted when ε is small, which is normal for explicit time discretizations. With implicit rotation term, c.f. (68), using the inverse R^{-1} of the rotation matrix R in the flux equations,

$$R = \begin{pmatrix} \frac{\varepsilon}{\Delta t} & -1 \\ 1 & \frac{\varepsilon}{\Delta t} \end{pmatrix} , \qquad R^{-1} = \frac{1}{1+(\varepsilon/\Delta t)^2} \begin{pmatrix} \frac{\varepsilon}{\Delta t} & 1 \\ -1 & \frac{\varepsilon}{\Delta t} \end{pmatrix} , \tag{73}$$

we find one eigenvalue of $A(\xi,\eta)$ to be

$$\lambda_3(\xi,\eta) = \frac{1}{2}[\cos(\xi\Delta x) + \cos(\eta\Delta y)] \qquad \Longrightarrow \qquad |\lambda_3| \le 1 . \tag{74}$$

The other two eigenvalues can be estimated to

$$\begin{aligned} |\lambda_{1,2}(\xi,\eta)|^2 \le \frac{\varepsilon}{\varepsilon^2+(\Delta t)^2} \Bigg[& \frac{\varepsilon}{2}\cos^2(\xi\Delta x) + \left(\frac{\Delta t}{\Delta x}\right)^2 \sin^2(\xi\Delta x) \\ & + \frac{\varepsilon}{2}\cos^2(\eta\Delta y) + \left(\frac{\Delta t}{\Delta y}\right)^2 \sin^2(\eta\Delta y) \Bigg] \\ \le \frac{\varepsilon}{\varepsilon^2+(\Delta t)^2} & \left\{ \max\left[\frac{\varepsilon}{2}, \left(\frac{\Delta t}{\Delta x}\right)^2\right] + \max\left[\frac{\varepsilon}{2}, \left(\frac{\Delta t}{\Delta y}\right)^2\right] \right\} . \end{aligned} \tag{75}$$

Consider first

$$\text{case 1:} \qquad \left(\frac{\Delta t}{\Delta x}\right)^2 < \frac{\varepsilon}{2} \qquad \text{and} \qquad \left(\frac{\Delta t}{\Delta y}\right)^2 < \frac{\varepsilon}{2} . \tag{76}$$

Clearly one has $|\lambda_{1,2}(\xi,\eta)|^2 < 1$ but the time step is restricted by ε. In fact we obtained the CFL-condition (72) without the restriction due to the rotation term, thus $\Delta t \sim \sqrt{\varepsilon}$. However, stability can be obtained also for

$$\text{case 2:} \qquad \left(\frac{\Delta t}{\Delta x}\right)^2 > \frac{\varepsilon}{2} \qquad \text{and} \qquad \left(\frac{\Delta t}{\Delta y}\right)^2 > \frac{\varepsilon}{2} . \tag{77}$$

Then, from (75) we get

$$(\Delta t)^2(\gamma^\varepsilon - 1) < \varepsilon^2 , \qquad \gamma^\varepsilon := \frac{\varepsilon}{(\Delta x)^2} + \frac{\varepsilon}{(\Delta y)^2} . \tag{78}$$

For $\gamma^\varepsilon < 1$ this relation holds for all ε and Δt; in this case there is no restriction on the time step. This is true in particular for $\varepsilon \to 0$ and thus shows the importance of implicit discretization of the rotation term (**B**-field term) in our AP scheme. On the other hand, for $\gamma^\varepsilon > 1$ we have the CFL-condition

$$\Delta t < \frac{\varepsilon}{\sqrt{\gamma^\varepsilon - 1}} . \tag{79}$$

This condition can be restrictive in an intermediate ε-regime, i.e. when $(\Delta x)^2 < \varepsilon \ll 1$. Remark in particular that for $\varepsilon \approx \Delta t$ equation (79) yields a CFL-condition of parabolic type,

$$\Delta t < \frac{2}{1/(\Delta x)^2 + 1/(\Delta y)^2}\,. \tag{80}$$

In the mixed case,

$$\text{case 3:} \qquad \left(\frac{\Delta t}{\Delta x}\right)^2 > \frac{\varepsilon}{2} \qquad \text{and} \qquad \left(\frac{\Delta t}{\Delta y}\right)^2 < \frac{\varepsilon}{2}\,, \tag{81}$$

we obtain, similar to the CFL-condition (79),

$$\Delta t < \frac{\varepsilon}{\sqrt{\gamma^\varepsilon - 2}}\,, \qquad \gamma^\varepsilon = \frac{2\varepsilon}{\Delta x^2}\,. \tag{82}$$

The different CFL-conditions (66), (79) and (82) have been taken into account in our (AP)-scheme as follows: first, we calculate the value of γ^ε for the given space mesh and ε. Then we choose the time step via

$$(\Delta t)_m = \begin{cases} \min(\Delta t_{RUS}, \Delta t_{ROT}) & \text{if} \quad \gamma^\varepsilon > 1\,, \\ \Delta t_{RUS} & \text{if} \quad \gamma^\varepsilon < 1\,, \end{cases} \tag{83}$$

where we computed Δt_{RUS} from (66) and Δt_{ROT} from (79) or from (82), respectively, with a CFL-number 0.5.

5. Numerical tests

We now start the verification process of the new (AP)-scheme. In a first part we will test our scheme regarding cyclotron modes, in order to show the capability of resolving fast plasma dynamics. We then discuss the dispersion relation issued from perturbations of an equilibrium with a temperature gradient in x. Due to this temperature gradient, yz-modes may grow in the plasma, so-called ion-temperature-gradient (ITG) modes, fact which we will use to test the (AP)-scheme against the ITG-dispersion relation, in particular growth rates. Finally, we shall explore the solutions obtained in the drift limit $\varepsilon \to 0$, a regime that is made accessible with our (AP)-scheme, thus showing its unique capability of resolving all plasma time scales.

Throughout the verification process, we set $L_x = 1$ and $L_y = 2$ to define the perpendicular plane (the domain size L_z can vary for different tests and is indicated in the respective section). Dispersion relations will be tested via the Fourier transform of the time signal arriving in the point $\mathbf{x}_o = (L_x/2, L_y/2, L_z/2)$. Let $s(t)$ stand for such a signal measured at this point, then its Fourier transform is denoted by $\hat{s}(\omega)$. The power (Fourier) spectrum is then labeled as $A_\omega := |\hat{s}(\omega)|^2$.

5.1. **Cyclotron waves.** Let us start with the verification of the fast plasma dynamics, namely the cyclotron waves. In our scaling, the two cyclotron frequencies are

$$\omega = \pm\omega_c = \pm\frac{1}{\varepsilon}\,. \tag{84}$$

We set $L_z = 10$ and chose the constant initial profiles

$$n_0 = 1\,, \qquad \Gamma_{x,0} = 10^{-2}\,, \qquad \Gamma_{y,0} = \Gamma_{z,0} = 0\,, \qquad T_0 = T_e = 1\,, \qquad \phi_0 = 0\,. \tag{85}$$

Due to the absence of spatial gradients we shall observe only the pure cyclotron frequencies (84), provided the time step Δt is small enough. Instead of the CFL-condition (83) we shall use a fixed time step which provides the necessary resolution, i.e. $\Delta t = 0.2\,\varepsilon$. The number of mesh points in each direction is $N_x = N_y = N_z = 20$. Power spectra and absolute values of signals $s(t) = \Gamma_x(t, \mathbf{x}_o)$ for runs with $\varepsilon \in \{10^{-2}, 10^{-3}, 10^{-4}, 10^{-5}, 10^{-6}, 10^{-7}, 10^{-8}\}$ are shown in Figure 1. Since the time step is decreased with ε, the cyclotron waves are resolved

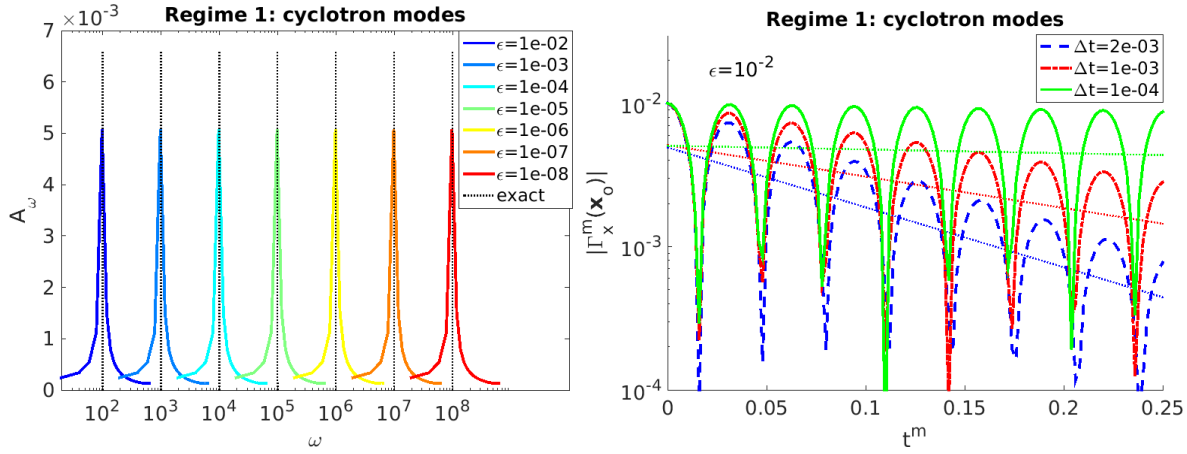

FIGURE 1. Simulation of cyclotron modes with the initial conditions (85). Left: power spectra A_ω for signals $s(t) = \Gamma_x(t, \mathbf{x}_o)$ obtained with an ε-dependent time step. Right: absolute value of $s(t)$ for $\varepsilon = 10^{-2}$ and different time steps Δt.

as $\varepsilon \to 0$. For $\varepsilon = 0.01$, the absolute values of the signals $s(t)$ obtained with three different time steps are observed in the right panel of Figure 1. Remark the damping of the signals (negative slope), which vanishes as $\Delta t \to 0$ and which is thus a numerical damping. This is easily understood from our discretization of the Lorentz-force term:

$$\boldsymbol{\Gamma}_\perp^{m+1} - \boldsymbol{\Gamma}_\perp^{m} = \frac{\Delta t}{\varepsilon}\,\boldsymbol{\Gamma}_\perp^{m+1} \times \mathbf{b}\,. \tag{86}$$

Scalar multiplication by $(\boldsymbol{\Gamma}_\perp^{m+1} + \boldsymbol{\Gamma}_\perp^{m})$ shows that

$$|\boldsymbol{\Gamma}_\perp^{m+1}|^2 - |\boldsymbol{\Gamma}_\perp^{m}|^2 = \frac{\Delta t}{\varepsilon}(\boldsymbol{\Gamma}_\perp^{m+1} \times \mathbf{b}) \cdot \boldsymbol{\Gamma}_\perp^{m} = -\frac{\Delta t^2}{\Delta t^2 + \varepsilon^2}|\boldsymbol{\Gamma}_\perp^{m}|^2 < 0\,. \tag{87}$$

The damping of cyclotron waves could be eliminated by using a Cranck-Nicholson discretization instead of (86). This question, and more generally the derivation of higher order numerical methods, is deferred to a future work.

5.2. **ITG modes.** Let us now perform some more challenging simulations, involving spatial gradients. For this, we choose the following equilibrium state of the (EL)-system (1), denoted with a subscript 'c':

$$n_c = 1\,, \qquad \mathbf{\Gamma}_c = \begin{pmatrix} 0 \\ v^* \\ 0 \end{pmatrix}\,, \qquad T_c(x) = T_e(x) = T_l + v^* x\,, \qquad \phi_c = 0\,. \tag{88}$$

Here, v^* stands for a constant drift velocity and T_l is the fixed temperature at $x = 0$. In

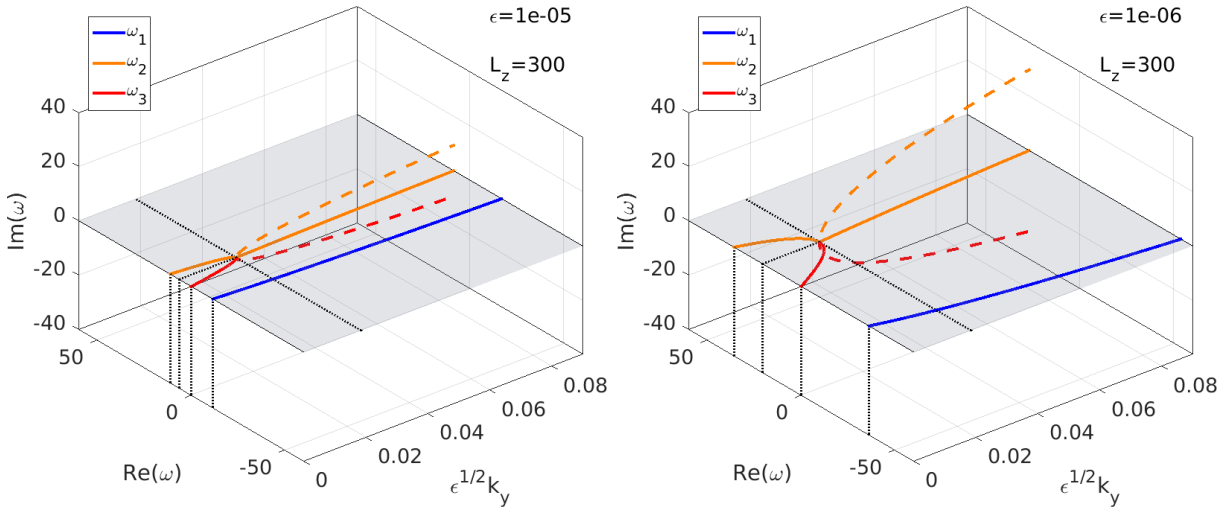

FIGURE 2. Solutions of the ITG dispersion relation (90) as functions of $\varepsilon^{1/2}k_y$ for $\varepsilon = 10^{-5}$ (left) and for $\varepsilon = 10^{-6}$ (right) with $|v^*| = 2$, $k_z = 2\pi/300$, $T_e = 2$ and $T_c = 2$. The instability threshold stated in (91) occurs where the imaginary part of ω becomes non-zero, indicated by the dashed lines emerging from the plane $Im(\omega) = 0$.

the following simulations we slightly perturb the equilibrium (88) at $t = 0$, i.e. we set

$$\begin{aligned} n_0 &= n_c + 10^{-4}\cos\left(m_y \frac{2\pi}{L_y} y + \frac{2\pi}{L_z} z\right) \exp\left(\frac{-(x - L_x/2)^2}{0.01}\right), \\ \mathbf{\Gamma}_0 &= \mathbf{\Gamma}_c\,, \qquad T_0 = T_c\,, \qquad \phi_0 = 0\,, \end{aligned} \tag{89}$$

where m_y stands for the y-mode number (m_z is set to one). The reaction of the (EL)-system to small perturbations can be predicted from the ITG-dispersion relation. The dispersion relation is obtained by linearizing the system (1) with respect to the stationary state (88), assuming that $\mathbf{\Gamma}_\perp = \mathbf{\Gamma}_D + \mathcal{O}(\varepsilon)$, i.e. that one is close to the drift approximation

for the perpendicular flux. Going to Fourier space (injecting plane wave solutions) in the linearized system then yields the cubic dispersion relation

$$\omega^3 \frac{\varepsilon}{k_z^2} - \omega\Big(\frac{5}{3}T_c + T_e\Big) + \omega^* T_e = 0\,, \tag{90}$$

with the drift frequency $\omega^* := v^* k_y$. In order for (90) to have one real and two complex conjugate roots, the discriminant of the cubic equation must be negative. This leads to the condition

$$k_y > \frac{2}{3^{3/2}} \frac{\left(\frac{5}{3}T_c + T_e\right)^{3/2}}{|v^*|\,T_e} \frac{k_z}{\sqrt{\varepsilon}}\,. \tag{91}$$

Solutions of the cubic equation (90) are plotted along with the cyclotron frequencies (84) in Figure 2 as functions of $\varepsilon^{1/2} k_y$ for two different values of ε and for $|v^*| = 2$, $k_z = 2\pi/300$, $T_e = 2$ and $T_c = 2$. The threshold for instability (91) occurs where the imaginary part of ω becomes non-zero, indicated by the dashed lines emerging from the plane $Im(\omega) = 0$.

Remark 3. *In our setting k_z is quantized, with a minimum value of $2\pi/L_z$. According to* (91) *the instability occurs for $k_y \sim \varepsilon^{-1/2}$, i.e. when the wavelength of the perturbation is of the order of the Larmor radius, c.f. Eq.* (18)*. The quantization of k_z is a consequence of our simplifying assumption that the magnetic field is pointing in the z-direction, $\mathbf{B} = \mathbf{e}_z$. We remark that magnetic configurations in Tokamaks are much more complicated; field lines form helices, whose twists are indicated by the safety factor q, the number of times a field line travels around the toroidal direction while it performs one round in the shorter poloidal direction. In our case $q = \infty$ everywhere. For finite q, the quantization of $k_\parallel$ (k_z in our case) is revoked and there are regions in the Tokamak where $k_\parallel \approx 0$. In this situation unstable ITG modes can occur even for large scale perturbations, $k_\perp \sim \mathcal{O}(1)$ (k_y in our case) . The generalization of the here presented AP-scheme to this situation will be the topic of a future work, for which the present paper serves as a basis.*

In what follows we set $T_l = 3$ and $v^* = -2$. First, the evolution of the system initialized thanks to (88)-(89) is simulated. We show the three-dimensional evolution of the density n in one situation below the instability threshold (91), c.f. Figure 3, and in one above the instability threshold, c.f. Figure 4. Below the threshold, a multitude of waves occur from the initial state $(m_y, m_z) = (2, 1)$, oscillating with the cyclotron- as well as the ITG frequencies. The density is not concentrated around its initial maximum at $x = L_x/2$, but touches the domain boundaries $x = 0$ and $x = L_x$ after short times. The amplitude of the initial wave has decreased at $t = 0.06$ due to the numerical diffusion in the Rusanov scheme[2]. The situation is different in Figure 4, where the amplitude of the signal is clearly growing over time for the mode $(m_y, m_z) = (5, 1)$. On top of that, the density is concentrated around its initial maximum at $x = L_x/2$, and only at the start of the non-linear phase, at $t = 2$ in the figure, begins to evolve towards the x-boundaries. Cyclotron modes

[2]Remark that no physical diffusion is present in the considered Euler-Lorentz system.

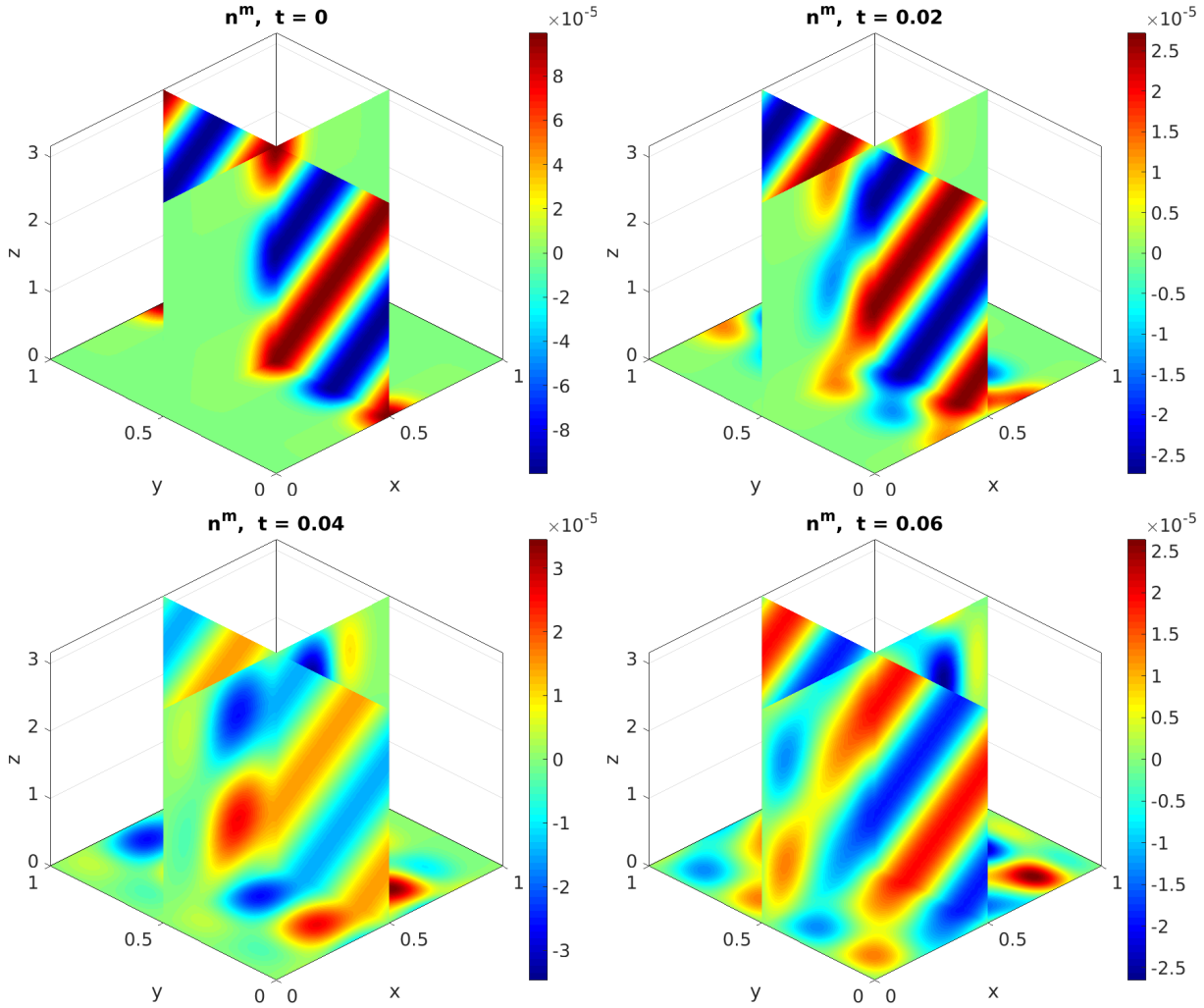

FIGURE 3. Evolution of the density n below the instability threshold, here for the mode $(m_y, m_z) = (2, 1)$ with parameters $\varepsilon = 0.1$, $L_x = L_y = 1$, $L_z = 3$, $N_x = N_y = 100$, $N_z = 20$.

are completely suppressed in this situation and only frequencies of the ITG-dispersion relation appear.

Our second task is to verify in more detail the (AP)-scheme by means of the dispersion relation (90). We use a space grid with $(N_x, N_y, N_z) = (40, 200, 20)$ and remind the reader that the time step is computed from the CFL-condition (83). We ran two series of simulations: in the first series we set $\varepsilon = 10^{-5}$, $L_z = 100$ and initialized separate runs with y-modes $m_y \in \{1, 2, 3, 5, 7, 8\}$ $(m_z = 1)$. In the second series we set $\varepsilon = 10^{-5}$, $L_z = 300$ and initialized with the y-modes $m_y \in \{1, 2, 3, 4, 5, 6\}$ $(m_z = 1)$. The simulated signals $s(t) = n(t, \mathbf{x}_o)$ and their corresponding Fourier spectra are depicted in Figures 5 and 6.

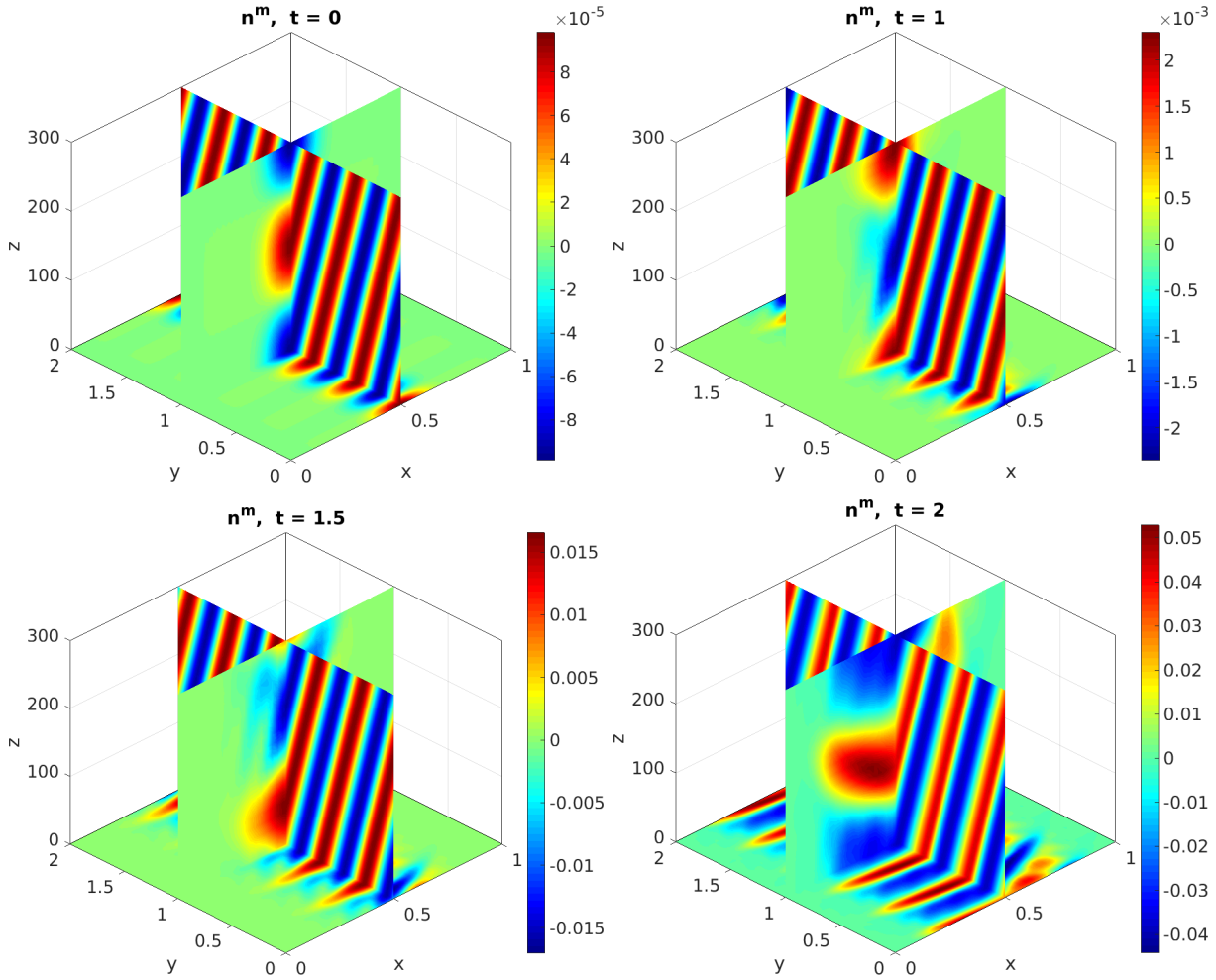

FIGURE 4. Evolution of the density n above the instability threshold, here for the mode $(m_y, m_z) = (5, 1)$ with parameters $\varepsilon = 10^{-5}$, $L_x = 1$, $L_y = 2$, $L_z = 300$, $N_x = 40$, $N_y = 200$, $N_z = 20$.

In the plots of the Fourier spectra (each spectrum corresponds to the respective signal above), the exact ITG frequencies issued from the dispersion relation (90) are shown as well (dashed lines). A good agreement between theory and simulation is observed in Figure 5. We remark that no growing mode occurs; all parameter sets lie below the instability threshold. On the contrary, one observes a damping of the signals, which is due to numerical diffusion in the Rusanov scheme, c.f. the fluxes (62). The agreement with theory is also good in Figure 6; here, however, one observes growing modes for $m_y \geq 3$. In the corresponding Fourier spectra only one peak is observed. This is because the amplitudes of the other two branches of the dispersion relation are negligible compared to the growing branch. The frequency of the growing branch is in almost perfect agreement with theory.

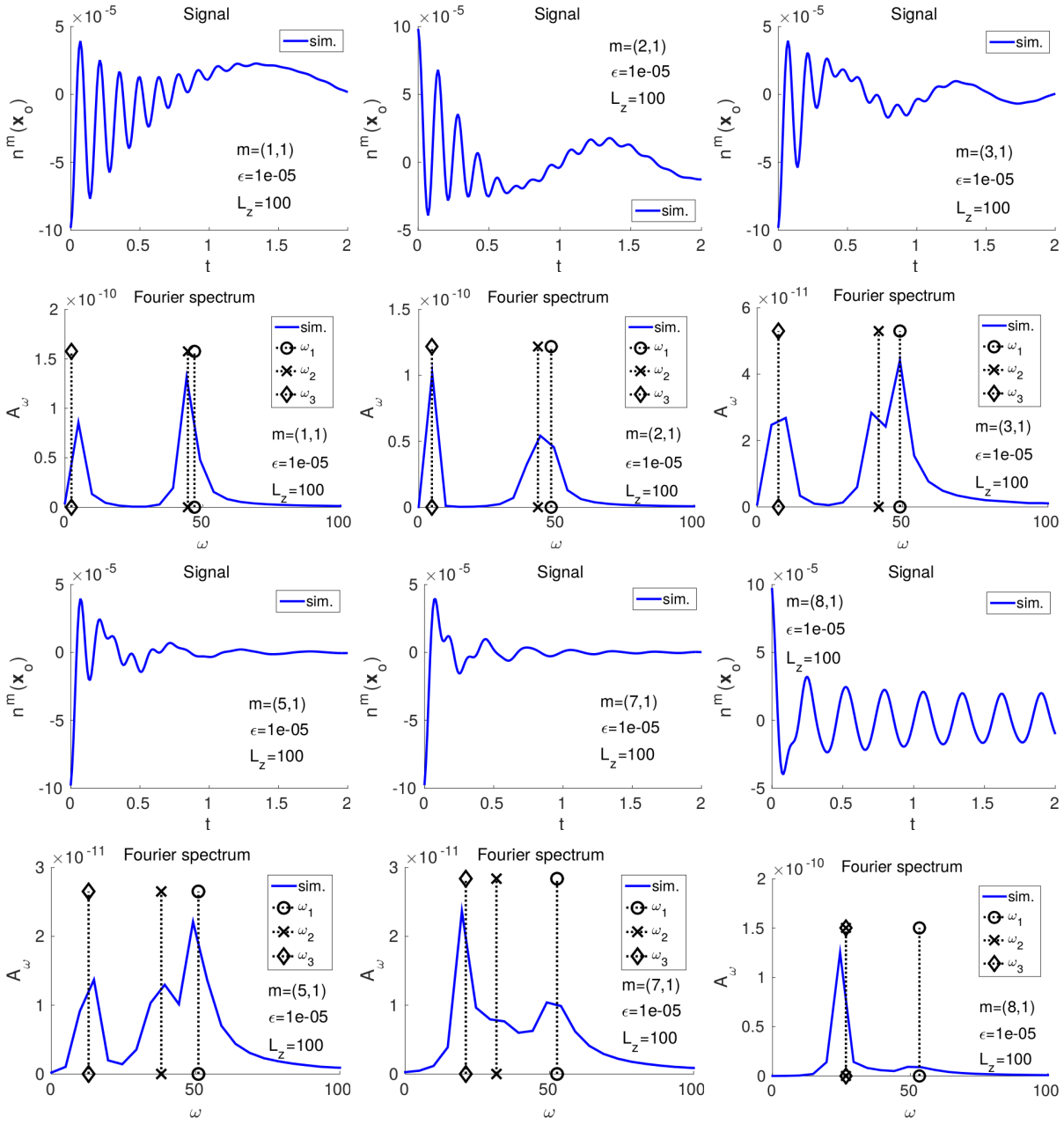

FIGURE 5. Signals $s(t) = n(t, \mathbf{x}_o)$ (subplot-lines one and three) and corresponding Fourier spectra (to the respective signals above) simulated with $\varepsilon = 10^{-5}$, $L_z = 100$ and $(N_x, N_y, N_z) = (40, 200, 20)$ for different modes $(m_y, 1)$. The dashed lines in the plots of the Fourier spectra show the exact ITG frequencies computed from (90).

Finally, we compare the simulated growth rates to their theoretical values. This is done for the parameter sets $(\varepsilon = 10^{-5}, L_z = 300)$ and $(\varepsilon = 10^{-6}, L_z = 1000)$ in Figure

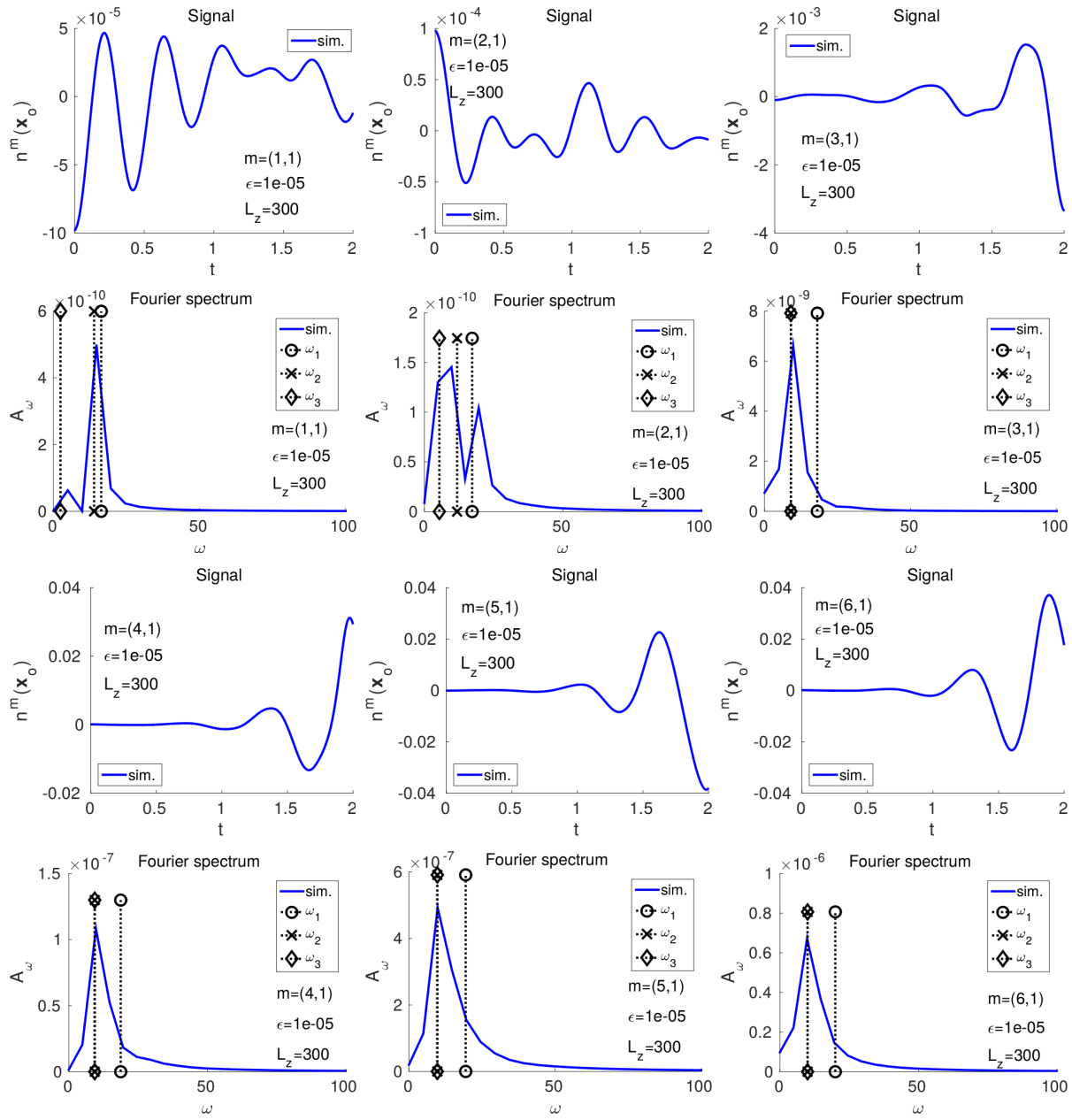

FIGURE 6. Signals $s(t) = n(t, \mathbf{x}_o)$ (subplots in lines one and three) and corresponding Fourier spectra (to the respective signals above) simulated with $\varepsilon = 10^{-5}$, $L_z = 300$ and $(N_x, N_y, N_z) = (40, 200, 20)$ for different modes $(m_y, 1)$. The dashed lines in the plots of the Fourier spectra show the exact ITG frequencies computed from (90).

7. Only the growing branch ($Im(\omega) > 0$) is found in the simulations, the amplitudes of the decreasing branch are too small in comparison. Remark that the first parameter set

(left subplot) corresponds to the signals shown in Figure 6. We see that the instability threshold is reproduced accurately, i.e. the imaginary part of ω is zero (or even negative due to numerical damping) below the theoretical threshold. The discrepancy with the theoretical growth rates for large wave numbers $k_y \gg 1$ is due to the numerical diffusion. Finer spatial resolution is required in order to reduce the numerical diffusion, which in turn leads to increased computational cost.

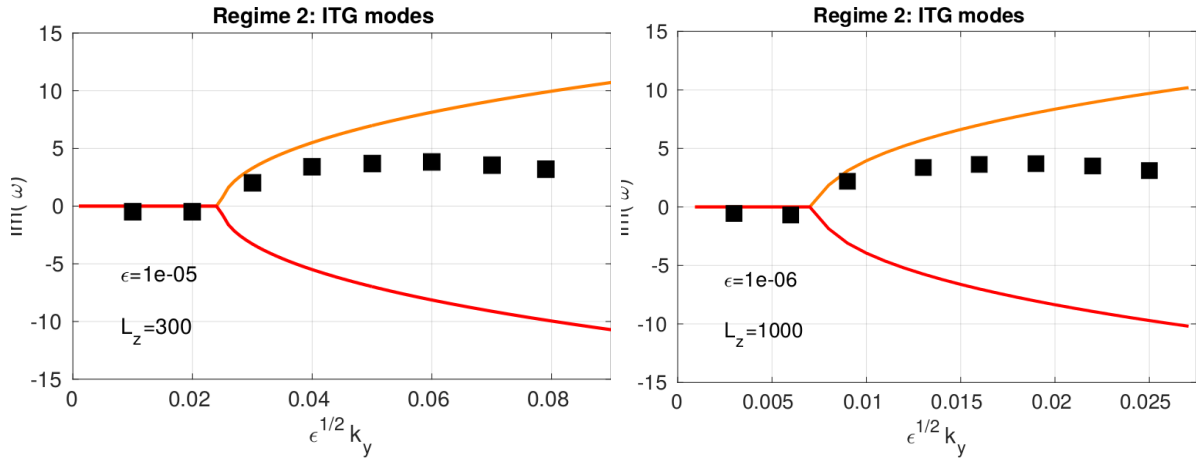

FIGURE 7. Comparison of the simulated growth rates (black squares) with the theoretical values issued from the dispersion relation (90) (solid lines). Only the growing branch ($Im(\omega) > 0$) is found in the simulations, the amplitudes of the decreasing branch are too small in comparison.

5.3. **Drift waves.** In our last series of tests we set ε equal to zero and take full advantage of the AP-property of our scheme. In this regime, the dispersion relation (90) yields the drift frequency

$$\omega_0 := \omega^* \frac{T_e}{\frac{5}{3}T_c + T_e}\,. \tag{92}$$

Simulations were carried out on the space mesh $40 \times 200 \times 20$ with the time step computed from (83). Results of runs with different mode numbers m_y are depicted in Figure 8. In the signals $s(t) = n(t, \mathbf{x}_o)$ on the left panel we remark a boundary layer at $t = 0$; in the drift limit, the scheme immediately restores the force balance in the z-direction as well as the drift-approximation in the perpendicular plane, leading to the boundary layer for ill-prepared initial conditions. In the right panel we observe good agreement between the simulated drift-wave frequencies and the theoretical value ω_0.

6. CONCLUSION

Fluid models are an important tool for the study of large scale plasma phenomena in fusion devices such as tokamaks. This work demonstrates that all-scale (all-speed) numerical schemes are possible for the plasma fluid equations with Braginskii closure. Our

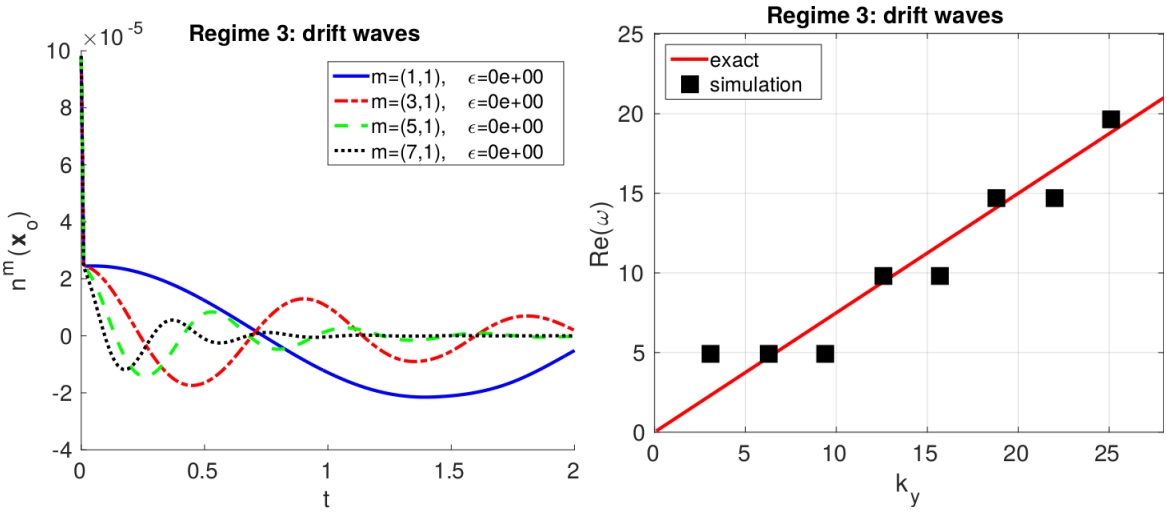

FIGURE 8. Simulation results in the regime $\varepsilon \to 0$. Left: signals $s(t) = n(t, \mathbf{x}_o)$ in the drift limit for different modes $(m_y, 1)$. Remark the boundary layer at $t = 0$. Right: comparison of simulated frequencies (black squares) with the theoretical value ω_0 (solid line).

asymptotic-preserving scheme is shown to correctly describe fast cyclotron waves on one end and low-frequency drift waves on the other end of the spectrum. The correct description of growing ITG modes has been demonstrated as well. The core of the scheme is an a priori reformulation of the flux conservation law, which permits the correct computation of the parallel flux in the drift limit. Future tasks involve the generalization of the code to more complex geometries, with the aim to approach realistic, global tokamak simulations.

Acknowledgments. This work has been carried out within the framework of the EUROfusion Consortium and has received funding from the Euratom research and training programme 2014-2018 under grant agreement No 633053. The views and opinions expressed herein do not necessarily reflect those of the European Commission.
Furthermore, the authors would like to acknowledge support of the"Agence Nationale de la Recherche" (ANR) in the frame of the contract BOOST (Building the future Of numerical methOdS for iTer) and from the ANR MOONRISE (MOdels, Oscillations and NumeRIcal SchEmes) under the reference number ANR-14-CE23-0007.

REFERENCES

[1] A. Arakawa, *Computational design for long-term numerical integration of the equations of fluid motion: two-dimensional incompressible flow. Part I*, Journal of Computational Physics **135** (1997) 103–114.
[2] M.A. Beer and G.W. Hammett, *Toroidal gyrofluid equations for simulations of tokamak turbulence*, Physics of Plasmas (1994-present) 3.11 (1996): 4046-4064.
[3] C. Besse, F. Deluzet, C. Negulescu and C. Yang, *Efficient numerical methods for strongly anisotropic elliptic equations*, Journal of Scientific Computing, 55(1) (2013), 231-254.

[4] S.I. Braginskii, *Transport processes in a plasma*, Reviews of plasma physics 1 (1965): 205.
[5] A.J. Brizard and T.S. Hahm, *Foundations of nonlinear gyrokinetic theory*, Reviews of modern physics 79.2 (2007): 421.
[6] S. Brull, P. Degond, and F. Deluzet, *Degenerate anisotropic elliptic problems and magnetized plasma simulations*, Communications in Computational Physics, 11(1) :147178, 2012.
[7] S. Brull, P. Degond, F. Deluzet and A. Mouton, *An asymptotic preserving scheme for a bifluid Euler-Lorentz system*, Kinetic and related models, 4 (2011), 10-40.
[8] S. Brull, F. Deluzet, and A. Mouton, *Numerical resolution of an anisotropic non-linear diffusion problem*, Communications in Mathema- tical Sciences, 13(1) :203224, 2015.
[9] F. Cordier, P. Degond, A. Kumbaroa, *An Asymptotic-Preserving all-speed scheme for the Euler and NavierStokes equations*, Journal of Computational Physics, 231(17), 56855704, 2012
[10] S.C. Cowley, R.M. Kulsrud and R. Sudan, *Considerations of ion-temperature-gradient-driven turbulence*, Physics of Fluids B: Plasma Physics, 3(10), (1991), 2767-2782.
[11] P. Crispel, P. Degond and M.-H. Vignal, *An asymptotically stable discretization for the EulerPoisson system in the quasi-neutral limit*, Comptes Rendus Mathematique 341.5 (2005): 323-328.
[12] P. Crispel, P. Degond and M.-H. Vignal, *An asymptotic preserving scheme for the two-fluid Euler-Poisson model in the quasineutral limit*, Journal of Computational Physics 223.1 (2007): 208-234.
[13] N. Crouseilles, P. Glanc, S. Hirstoaga, E. Madaule, M. Mehrenberger, J. Ptri, *A new fully two-dimensional conservative semi-Lagrangian method: applications on polar grids, from diocotron instability to ITG turbulence*, Eur. Phys. J. D, 68 11, p. 252, (2014).
[14] N. Crouseilles, M. Kuhn, and G. Latu. *Comparison of numerical solvers for anisotropic diffusion equations arising in plasma physics*, Journal of Scientific Computing, pp.1-38, 2015.
[15] N. Crouseilles, M. Lemou, *An asymptotic preserving scheme based on a micro-macro decomposition for collisional Vlasov equations: diffusion and high-field scaling limits*, Kinetic Related Models, 4, pp. 441-477, (2011).
[16] N. Crouseilles, M. Lemou, F. Méhats, *Asymptotic preserving schemes for highly oscillatory kinetic equations*, J. Comput. Phys., 248, pp.287-308, (2013).
[17] P. Degond, *Asymptotic-preserving schemes for fluid models of plasmas*, arXiv preprint arXiv:1104.1869 (2011).
[18] P. Degond, F. Deluzet and C. Negulescu, *An asymptotic preserving scheme for strongly anisotropic elliptic problems*, Multiscale Modeling & Simulation 8.2 (2010): 645-666.
[19] P. Degond, F. Deluzet, A. Sangam and M.-H. Vignal, *An asymptotic preserving scheme for the Euler equations in a strong magnetic field*, Journal of Computational Physics, 228(10) (2009), 3540-3558.
[20] P. Degond, F. Deluzet and D. Savelief, *Numerical approximation of the Euler-Maxwell model in the quasineutral limit*, Journal of Computational Physics 231.4 (2012): 1917-1946.
[21] P. Degond, H. Liu, D. Savelief and M.-H. Vignal, *Numerical approximation of the Euler-Poisson-Boltzmann model in the quasineutral limit*, Journal of Scientific Computing, 51(1) (2012), 59-86.
[22] P. Degond, J.-G. Liu and M.-H. Vignal, *Analysis of an asymptotic preserving scheme for the Euler-Poisson system in the quasineutral limit*, SIAM Journal on Numerical Analysis 46.3 (2008): 1298-1322.
[23] P. Degond, A. Lozinski, J. Narski, J. and C. Negulescu, *An asymptotic-preserving method for highly anisotropic elliptic equations based on a micro-macro decomposition*, Journal of Computational Physics, 231(7) (2012), 2724-2740.
[24] F. Deluzet, C. Negulescu, M. Ottaviani and S. Possanner, *Numerical study of the plasma tearing instability on the resistive time scale*, Journal of Computational Physics, Volume 280, 1 January 2015, Pages 602-625.
[25] P. Degond, M. Tang, *All speed method for the Euler equation in the low mach number limit*, Communications in Computational Physics, 10,1-31,2011.
[26] G. Dimarco, L. Pareschi, *Asymptotic preserving Implicit-Explicit Runge-Kutta methods for nonlinear kinetic equations*, SIAM J. Numer. Anal. 51, 1064-1087, (2013).

[27] W. Dorland and G. W. Hammett, *Gyrofluid turbulence models with kinetic effects*, Physics of Fluids B: Plasma Physics (1989-1993) 5.3 (1993): 812-835.
[28] G.L. Falchetto and M. Ottaviani, *Effect of collisional zonal-flow damping on flux-driven turbulent transport*, Physical review letters 92.2 (2004): 025002.
[29] F. Filbet, S. Jin, *A class of asymptotic preserving schemes for kinetic equations and related problems with stiff sources*, J. Comp. Phys. 2, pp. 7625–7648 (2010).
[30] F. Filbet, A. Rambaud, *Analysis of an Asymptotic Preserving Scheme for Relaxation Systems*, ESAIM - Math. Mod. Num. Anal. vol. 47, pp. 609–633, 2013
[31] X. Garbet et al., *Global simulations of ion turbulence with magnetic shear reversal*, Physics of Plasmas (1994-present) 8.6 (2001): 2793-2803.
[32] J.P. Goedbloed and S. Poedts, *Principles of magnetohydrodynamics: with applications to laboratory and astrophysical plasmas*, Cambridge university press, 2004.
[33] G.W. Hammett, M.A. Beer, W. Dorland, S.C. Cowley and S.A. Smith, *Developments in the gyrofluid approach to tokamak turbulence simulations*, Plasma physics and controlled fusion, 35(8) (1993), 973.
[34] R.D. Hazeltine and J.D. Meiss, *Plasma confinement*, Courier Dover Publications, 2003.
[35] J.D. Huba, *NRL: plasma formulary*, No. NRL/PU/6790–04-477. NAVAL RESEARCH LAB WASHINGTON DC BEAM PHYSICS BRANCH, 2004.
[36] S. Jin, *Asymptotic preserving (AP) schemes for multiscale kinetic and hyperbolic equations: a review*, Lecture Notes for Summer School on Methods and Models of Kinetic Theory), Porto Ercole (Grosseto, Italy) (2010).
[37] S. Jin, *Efficient asymptotic-preserving (AP) schemes for some multiscale kinetic equations*, SIAM J. Sci. Comput., 21(2) :441454, 1999.
[38] I. Langmuir. *The interaction of electron and positive ion space charges in cathode sheaths*, Physical Review, 33(6):954989, 1929.
[39] R.J. LeVeque, *Finite volume methods for hyperbolic problems*, Vol. 31. Cambridge university press, 2002.
[40] J. Narski and M. Ottaviani. *Asymptotic Preserving scheme for strongly anisotropic parabolic equations for arbitrary anisotropy direction*, Computer Physics Communications, 185(12) :31893203, 2014.
[41] C. Negulescu and S. Possanner, *Closure of the strongly-magnetized electron fluid equations in the adiabatic regime*, submitted to MMS (SIAM).
[42] V. Grandgirard et al., *A drift-kinetic semi-Lagrangian 4D code for ion turbulence simulation*, Journal of Computational Physics, 217(2), (2006), 395-423.
[43] W. Horton and R.D. Estes, *Fluid simulation of ion pressure gradient driven drift modes*, Plasma Physics, 22(7), (1980), 663.
[44] L. Pareschi, G. Russo, *Efficient asymptotic preserving deterministic methods for the Boltzmann equation*, AVT-194 RTO AVT/VKI, Models and Computational Methods for Rarefied Flows, Lecture Series held at the von Karman Institute, Rhode St. Gense, Belgium, 24 -28 January (2011).
[45] M. Tang, *Second order method for Isentropic Euler equation in the low Mach number regime*, Kinetic and Related Models, 5(1), 155-184, 2012.

*Université de Toulouse & CNRS, UPS, Institut de Mathématiques de Toulouse UMR 5219, F-31062 Toulouse, France.

†CEA Cadarache, IRFM/SCCP Bat. 513/148 13108 Saint-Paul-lez-Durance, France.
E-mail address: fabrice.deluzet@math.univ-toulouse.fr
E-mail address: Maurizio.Ottaviani@cea.fr
E-mail address: stefan.possanner@ipp.mpg.de